Article

Connectomes across development reveal principles of brain maturation

https://doi.org/10.1038/s41586-021-03778-8

Received: 21 May 2020

Accepted: 29 June 2021

Published online: 4 August 2021

Check for updates

Daniel Witvliet[1,2]✉, Ben Mulcahy[1,9], James K. Mitchell[3,4,9], Yaron Meirovitch[4,5], Daniel R. Berger[4], Yuelong Wu[4], Yufang Liu[1], Wan Xian Koh[1], Rajeev Parvathala[5], Douglas Holmyard[1], Richard L. Schalek[4], Nir Shavit[5], Andrew D. Chisholm[6], Jeff W. Lichtman[4,7]✉, Aravinthan D. T. Samuel[3,4]✉ & Mei Zhen[1,2,8]✉

An animal's nervous system changes as its body grows from birth to adulthood and its behaviours mature[1–8]. The form and extent of circuit remodelling across the connectome is unknown[3,9–15]. Here we used serial-section electron microscopy to reconstruct the full brain of eight isogenic *Caenorhabditis elegans* individuals across postnatal stages to investigate how it changes with age. The overall geometry of the brain is preserved from birth to adulthood, but substantial changes in chemical synaptic connectivity emerge on this consistent scaffold. Comparing connectomes between individuals reveals substantial differences in connectivity that make each brain partly unique. Comparing connectomes across maturation reveals consistent wiring changes between different neurons. These changes alter the strength of existing connections and create new connections. Collective changes in the network alter information processing. During development, the central decision-making circuitry is maintained, whereas sensory and motor pathways substantially remodel. With age, the brain becomes progressively more feedforward and discernibly modular. Thus developmental connectomics reveals principles that underlie brain maturation.

The developing nervous system faces many challenges. As the animal's anatomy changes and the environment fluctuates, some circuits, such as locomotion[1–3], maintain robust outputs. New circuits are constructed to support new functions, such as reproduction[4,5]. To adapt and learn, the nervous system modifies circuits in response to internal and external cues[6]. In many organisms, adaptive mechanisms have been identified that coincide with aspects of behavioural maturation[7,8] (Supplementary Discussion). However, the developmental principles that underlie the collective synaptic changes that shape the adult brain remain unknown.

Serial-section electron microscopy has been used to reconstruct neural circuits with synaptic resolution across species[3,9–15] (Supplementary Discussion). We leveraged advances in electron microscopy reconstruction to study the entire brain of *C. elegans*—its circumpharyngeal nerve ring and ventral ganglion—across development (Extended Data Fig. 1a, Methods). We fully reconstructed the brains of eight isogenic hermaphrodites at different postembryonic ages, from hatching (birth) to adulthood (Fig. 1a, Supplementary Fig. 1, Supplementary Videos 1, 2). For each developmental time point, we quantified the length, shape and position of every neural and muscle fibre in the nerve ring. We mapped every physical contact between all neurons and muscles, as well as every chemical synapse between neurons, muscles and glia to generate a connectome (Fig. 1b, Extended Data Fig. 2, Extended Data Table 1, Supplementary Tables 1–5; Methods). Our comparison of developmental connectomes reveals principles by which synaptic changes shape the brain of a developing worm.

Uniform growth and stable brain geometry

We found that uniform neurite growth maintains brain geometry. The shape and relative position of every neurite in the brain was largely established by birth (Extended Data Figs. 1b, 3). From birth to adulthood, the total length of neurites increased fivefold (Fig. 1c), similar to the fivefold increase in body length (from approximately 250 µm to 1,150 µm). Neurites grew proportionally (Extended Data Fig. 1b), maintaining physical contact between cells that were present at birth across maturation (Fig. 1d, Extended Data Fig. 1b) with a few exceptions (Supplementary Fig. 2, Supplementary Video 3). Thus, the brain grows uniformly in size and maintains its overall geometry without substantially changing the shape or relative position of neurites.

The total number of chemical synapses increased sixfold (from approximately 1,300 at birth to approximately 8,000 in adults) (Fig. 1e). Except for the first larval stage (L1), synapse number increased in proportion to neurite length, maintaining synapse density across development (Fig. 1f). The increase in synapse density during L1 coincided with an increase in left–right wiring symmetry (Extended Data Fig. 1d, e).

[1]Lunenfeld-Tanenbaum Research Institute, Mount Sinai Hospital, Toronto, Ontario, Canada. [2]Department of Molecular Genetics, University of Toronto, Toronto, Ontario, Canada. [3]Department of Physics, Harvard University, Cambridge, MA, USA. [4]Center for Brain Science, Harvard University, Cambridge, MA, USA. [5]Computer Science and Artificial Intelligence Laboratory, Massachusetts Institute of Technology, Cambridge, MA, USA. [6]Division of Biological Sciences, Section of Cell and Developmental Biology, University of California, San Diego, San Diego, CA, USA. [7]Department of Molecular and Cellular Biology, Harvard University, Cambridge, MA, USA. [8]Department of Physiology, University of Toronto, Toronto, Ontario, Canada. [9]These authors contributed equally: Ben Mulcahy, James K. Mitchell. ✉e-mail: daniel.witvliet@gmail.com; jeff@mcb.harvard.edu; samuel@physics.harvard.edu; meizhen@lunenfeld.ca

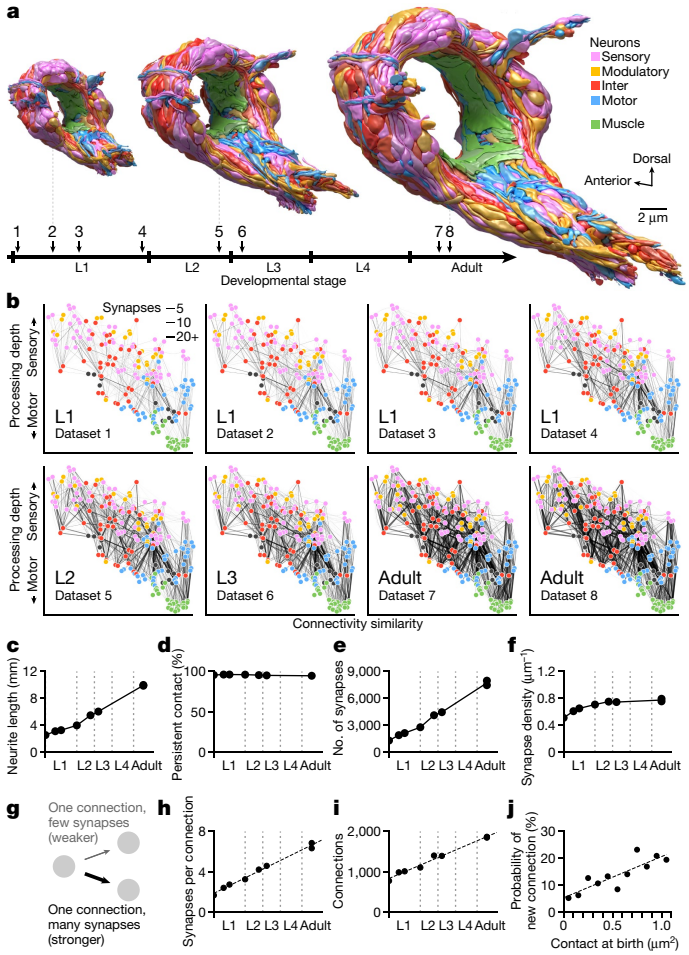

Fig. 1 | The developing brain maintains overall geometry with increasing numbers of synapses and connections. a, Developmental timeline of eight reconstructed individuals. Volumetric models of the brain, coloured by cell type, shown at three stages. **b**, Wiring diagrams for eight individuals. Each circle represents a cell. Each line represents a connection between two cells with at least one chemical synapse. The vertical axis denotes signalling from sensory perception (top) to motor actuation (bottom). The horizontal axis denotes connectivity similarity—neurons that share partners are positioned more closely[20]. Signal flow and connectivity similarity are based on accumulated connections from all datasets. **c**, Summed length of all neurites in each brain. **d**, Persistent physical contact—the summed physical contact between neurite pairs that exist at birth and persists into adulthood—accounts for nearly all contact areas at all stages. **e**, Total synapse numbers in each brain. **f**, Synapse density—the total number of synapses divided by total neurite length. **g**, Schematic of weak versus strong connections. Each connection contains at least one synapse between two cells. **h**, Mean number of synapses per connection existing from birth. **i**, Total number of connections in each brain. **j**, Probability of forming a new connection at physical contacts existing from birth. A connection is called new when it is absent in early L1 stages (datasets 1 and 2) and present in adults (datasets 7 and 8). ***$r = 0.87$, $P = 4.5 \times 10^{-4}$, two-sided Spearman's rank correlation.

In the adult, about 90% of neurons are left–right symmetric pairs in position, morphology and connectivity[9]. Some of these neurons exhibited left–right asymmetry in connectivity at birth (Extended Data Fig. 1d, e). One interpretation of early asymmetry is incompleteness: *C. elegans* hatches before the L1 connectome is made symmetric by adding synapses after birth.

Additional growth occurred as small spine-like protrusions along many neurites and muscle processes. The number of such protrusions increased fivefold after birth, contributing 17% of synapses in the adult connectome (Extended Data Fig. 4).

Non-uniform synapse addition

From birth to adulthood, we found that non-uniform synapse addition reshapes the connectome. New synapses create new connections and strengthen existing connections. We define a connection as a pair of cells connected by one or more chemical synapses (Fig. 1g). At birth, the 204 cells in the brain were interconnected by approximately 1,300 synapses among around 800 connections. Over maturation, approximately 4,500 new synapses strengthened most connections that were present at birth. The mean synapse number per connection increased from 1.7 at birth to 6.9 at adulthood (Fig. 1h). Approximately 1,200 new synapses formed new connections between previously non-connected cells, resulting in a 2.4-fold increase from the number of connections at birth (Fig. 1i).

Synapse addition did not occur uniformly across the brain. Preferential synapse addition occurred in multiple contexts. First, new connections were more likely to form between neurons that shared larger physical contact areas at birth (Fig. 1j). Thus, physical contacts at birth form a constant scaffold on which network formation unfolds.

Second, synapse addition preferentially strengthened inputs to 'hub' neurons, neurons that already exhibited more connections at birth (Extended Data Fig. 1f). Hub neurons disproportionately strengthened existing input connections over time and disproportionately established more new input connections. However, the number of outputs from hub neurons did not disproportionately increase (Extended Data Fig. 1g, h). Thus, maturation progressively focuses the flow of information to the most highly connected neurons at birth.

Third, synapse addition selectively strengthened a cell's individual connections. We found no correlation in the strengthening of existing input connections to each cell from different presynaptic partners, leading to divergence in the relative strengths of different inputs (Extended Data Fig. 1i–l). However, strengthening of the existing output connections from individual cells was correlated, thereby maintaining relative strengths during development (Extended Data Fig. 1k, l). Thus, each cell appears to regulate the strengthening of its outputs but not its inputs.

Unlike mammals, where synapse pruning is a hallmark of early development, we did not observe systematic synapse elimination. In the *C. elegans* brain, synaptic connections are rarely removed; instead, a diminished connection is mediated by selectively strengthening other connections.

Stereotyped and variable connections

We found that isogenic animals exhibited both stereotyped and variable connections. We mapped the change in synapse number for each connection across development, and thereby classified each connection as stable, developmentally dynamic or variable (Fig. 2a, Extended Data Fig. 5, Supplementary Table 6, Methods). Stable connections were present from birth to adulthood and maintained their relative strengths. Developmentally dynamic connections significantly increased or decreased their relative strengths in a stereotyped manner, sometimes forming new connections or more rarely eliminating connections at specific life stages. Variable connections exhibited no consistent trend in synapse number and were not present in every animal.

In the adult connectome, stable and variable connections each represented around 43% of total connections. Developmentally dynamic connections represented around 14% of connections (Fig. 2b). We observed similar partitions when connections were classified by synapse size (Extended Data Fig. 6a), suggesting that synapse number is a good proxy for synapse size.

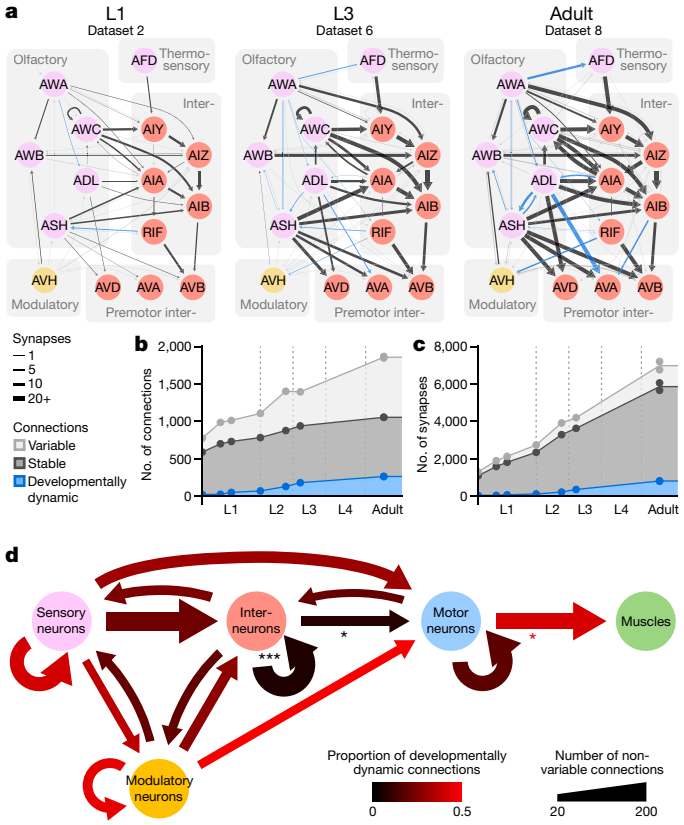

Fig. 2 | Connectomes of isogenic individuals include both stereotyped and variable connections. a, Example of a sensory sub-circuit across maturation. Circles represent cells, colour-coded by cell type. Lines indicate stable (black), developmentally dynamic (blue) and variable (grey) connections. **b**, Total number of stable, developmentally dynamic and variable connections across maturation. **c**, Total number of synapses in stable, developmentally dynamic and variable connections across maturation. **d**, Wiring diagram with invariant (stable and developmentally dynamic) connections between different cell types. Connections with statistically significantly different proportions of developmentally dynamic connections are denoted, $^{*}P = 3.2 \times 10^{-2}$ (motor–muscle), 4.2×10^{-2} (inter–motor), $^{***}P = 2.0 \times 10^{-5}$ (inter–inter), two-tailed *z*-test, false discovery rate (FDR)-adjusted using Benjamini–Hochberg correction ($n = 160$ (interneuron–interneuron), 52 (interneuron–motor neuron) and 145 (motor neuron–muscle) observations).

Stable connections contained more synapses than variable connections (6.6 ± 5.8 versus 1.4 ± 1.0 synapses per connection (mean ± s.d.), in adults), and constituted a large proportion (~72%) of total synapses (Fig. 2c). Nonetheless, variable connections were common. Similar to other connections, most variable connections formed at cell contacts that already existed at birth (Extended Data Figs. 3, 5, 6b). The prevalence of variable connections is not a result of serendipitous synapse annotation between adjacent neurites (Extended Data Fig. 6c–f).

Stable and developmentally dynamic connections represent the invariant portion of the connectome that is shared across individual worms. Variable connections represent the portion that is unique to each worm (Extended Data Fig. 6g–i). The proportion of variable connections differed according to cell type (Extended Data Fig. 6j). Modulatory neurons exhibited higher variability in their output connections, whereas motor neurons exhibited the least variability. The high stereotypy of connections from motor neurons to muscles may reflect high fidelity in circuits for motor execution. Modulatory neurons, which secrete monoamines and neuropeptides by volume release, may have less need for precisely positioned synaptic outputs.

Stable interneuron connections

Excluding variable connections enables assessment of developmental changes in connectivity that are shared across individuals. Developmentally dynamic connections were not uniformly distributed among cell types or circuit layers (Fig. 2d). Connections between interneurons and from interneurons to motor neurons had disproportionately more stable connections than developmentally dynamic connections (Fig. 2d, Extended Data Fig. 7a). By contrast, connections between and from sensory, modulatory and motor neurons had many developmentally dynamic connections (Fig. 2d, Extended Data Fig. 5). Spine-like protrusions may facilitate developmental changes, as developmentally dynamic connections were twice as likely to involve these protrusions than other connections (Extended Data Fig. 4h)

Thus, maturation changes how sensory information is integrated and relayed to downstream neurons. However, the layout of interneuron circuits, the core decision-making architecture, is largely stable from birth to adulthood.

Increases in feedforward signalling with age

We investigated how the sum of synaptic changes collectively alters the network structure. First, we examined how synaptic changes affect information flow. We classified connections from the sensory to motor layer as feedforward, connections from the motor to sensory layer as feedback, and connections between neurons of the same cell type as recurrent (Fig. 3a). Among stable connections, synapse addition strengthened existing feedforward connections more than feedback or recurrent connections (Extended Data Fig. 7b). Developmentally dynamic connections also preferentially increased feedforward signal flow (Extended Data Fig. 7c). Cumulatively, the proportion of synapses in feedforward connections gradually increased (Fig. 3b).

Thus, one global pattern of brain maturation augments signal flow from sensation to action, making the brain more reflexive with age.

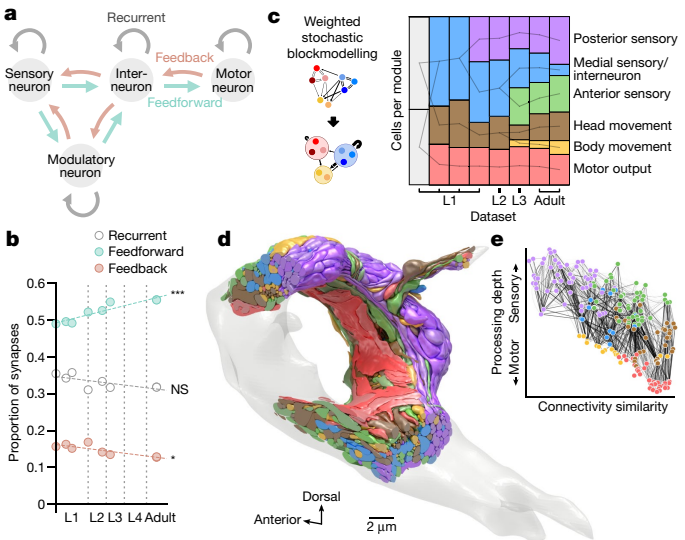

Fig. 3 | Developmental increase in feedforward signalling and modularity. a, Schematic of feedforward, feedback and recurrent connections defined by cell types. **b**, Proportions of the total number of synapses in feedforward, feedback and recurrent connections. $^{*}P = 0.017$, $^{***}P = 2.0 \times 10^{-4}$, NS, not significant ($P = 0.11$), Spearman's rank correlation, FDR-adjusted using Benjamini–Hochberg correction. **c**, Number of cells in each module across maturation, determined by weighted stochastic block modelling. Modules connected by a line share significant numbers of neurons. Supplementary Table 7 shows number of cells in each module. **d**, **e** Volumetric model (**d**) and wiring diagram (**e**) of the adult brain (dataset 8), colour-coded by module. Cell coordinates are represented as in Fig. 1b.

Modularity increases with age

Next, we compared the brain-wide community structure across maturation. We used weighted stochastic block modelling to group neurons of similar connectivity into distinct modules[16]. In the adult, modularity corresponds to six cellular congregations with distinct functions (Fig. 3c–e, Extended Data Fig. 8a, Supplementary Table 7). Sensory neurons and interneurons separate into three modules: anterior sensory (consisted of labial sensory neurons), posterior sensory (amphid sensory neurons and associated interneurons) and medial interneurons (other sensory neurons and most interneurons). Head motor neurons and descending premotor interneurons separate into two modules. Muscles constitute another module.

We discerned fewer modules at earlier developmental stages, starting with two modules at birth (Fig. 3c, Extended Data Fig. 8a, Supplementary Table 7). Most of the increase in modularity is owing to a small fraction of total synapses over development (Extended Data Fig. 8b). Seventy-four per cent of new synapses are added to stable connections that did not increase modularity. The increase in modularity is mostly owing to developmentally dynamic connections, which account for only 14% of new synapses. Notably, variable connections also contributed to module segregation.

After birth, an increase of connections further segregates closely connected neurons into more discernible modules (Fig. 3d, e, Supplementary Video 4). The physical proximity of neurons in these modules resembles distinct brain lobes with different functions.

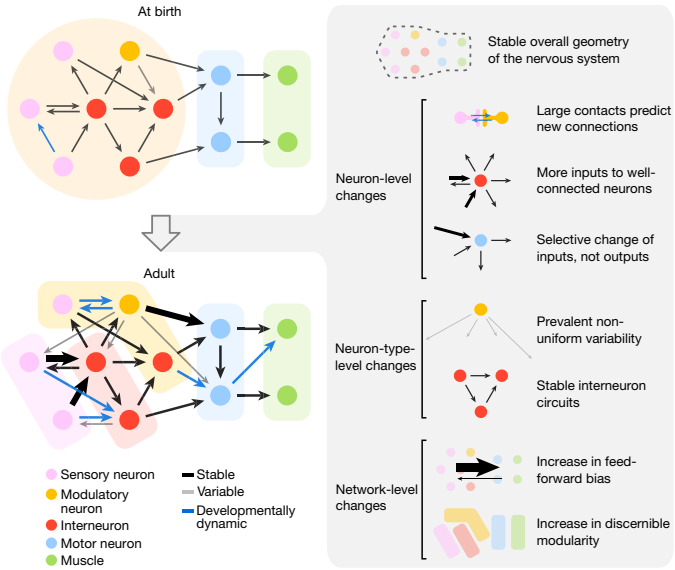

Fig. 4 | Developmental principles of brain maturation. Left, schematic of brain-wide synaptic changes from birth to adulthood. Right, principles of maturation describing synaptic changes at the level of brain geometry, individual neurons, neuron types and entire networks. Thicker lines represent stronger connections with more synapses.

Discussion

From birth to adulthood, the *C. elegans* brain enlarges sixfold in volume while preserving several features. Overall brain geometry, shape, relative placement of individual neurons and their physical contacts are surprisingly stable. Established neurite neighbourhoods at birth provide the structural platform that constrains and supports wiring maturation. However, changes in brain connectivity were not explained by uniform enlargement of existing wiring. With the fivefold increase in synapse number from birth to adulthood, synaptic changes were not distributed uniformly through the network. Rather, we uncovered several developmental patterns that shape how the brain's network changes (Fig. 4).

Large contacts predict new connections

Because the overall geometry of the brain is constant, physical contacts between neurites are nearly invariant across development. Most new synapses appear where physical contacts already exist, both adding synapses to connections between neurons and creating new connections between neurons. The larger the physical contact, the greater the probability of a new connection. The brain's geometry at birth creates the scaffold on which adult connectivity is built.

Hub neurons at birth get more inputs

Developmental synapse addition is not equal among neurons. Cells with larger numbers of connections at early stages receive disproportionately more new synapses, both strengthening existing input connections and creating new input connections. By contrast, these neurons add fewer synapses to output connections. Thus, well-connected neurons become better integrators of information, but not broader communicators of that information.

Convertent inputs undergo selective changes

Synapses selectively change the strengths of existing connections. The strengths of input connections that converge on the same neuron tend to become more heterogeneous. By contrast, the outputs from the same neuron maintain their relative strengths. Neurons thus become differentially driven by a subset of their presynaptic partners, but distribute that information uniformly among their postsynaptic partners.

The wiring diagram is not stereotyped

Each worm has connections that are not found in other individuals. About 43% of all cell–cell connections—accounting for 16% of all chemical synapses—are not conserved between isogenic individuals. By contrast, physical contacts between neurites at birth are maintained across developmental stages. Wiring variability contrasts with the assumption that the *C. elegans* connectome is hardwired.

Interneuron circuits are stable

Stable wiring between interneurons may constitute the decision-making architecture of the developing brain. Stability of the core parts of the nervous system implies that the central processing unit is robust enough to be used in different contexts. Maturation changes the flow of sensory information into the central processor and its motor readout without changing the central processor itself. Sensory maturation may reflect changes caused by learning and memory[17]. Motor circuit maturation may reflect adaptations to the changing musculature of the growing body[18].

Feedforward bias increases with age

Synaptogenesis preferentially creates new connections and strengthens existing connections in the direction from sensory to motor layers. This makes the network more feedforward over time. The adult brain, with increased feedforward-bias, may be more effective in rapid information processing and in reflexive decisions. The juvenile brain, which has more feedback connections, may have a greater capacity for learning and adaptation. Architecture in the adult brain may arise partly from feedback-mediated optimization of sensorimotor pathways.

Discernible modularity increases with age

Synapse remodelling that generates developmental and variable connections increases the modularity of the brain, making it possible to resolve more sub-networks for sensory or motor processing with maturation. In the adult brain, it becomes possible to resolve functional communities among cells that are physically close to one another

(Fig. 3d). These communities form spatially compact areas reminiscent of distinct brain areas in larger animals.

Perspective

In the *C. elegans* brain, synaptic remodelling from the cellular to network levels is likely to have functional consequences on behaviour. Most investigations of flexibility in neural circuits and behaviours focus on functional modulations of connectomes that are assumed to be anatomically static[19]. Our comparison of connectomes argues that the maturation and variability of brain and behaviour are not separated from the wiring changes. Comparative connectomics is needed to reveal the origin of similarities and differences in structure and behaviour within and across species. High-throughput electron microscopy establishes a foundation for understanding how genes, experience, and evolution create the behaving adult (Supplementary Discussion).

Online content

Any methods, additional references, Nature Research reporting summaries, source data, extended data, supplementary information, acknowledgements, peer review information; details of author contributions and competing interests; and statements of data and code availability are available at https://doi.org/10.1038/s41586-021-03778-8.

1. Bucher, D., Prinz, A. A. & Marder, E. Animal-to-animal variability in motor pattern production in adults and during growth. *J. Neurosci.* **25**, 1611–1619 (2005).
2. Kämper, G. & Murphey, R. Maturation of an insect nervous system: Constancy in the face of change. *Comp. Biochem. Physiol. A* **109**, 23–32 (1994).
3. Gerhard, S., Andrade, I., Fetter, R. D., Cardona, A. & Schneider-Mizell, C. M. Conserved neural circuit structure across *Drosophila* larval development revealed by comparative connectomics. *eLife* **6**, e29089 (2017).
4. Kagan, J., Herschkowitz, N. & Herschkowitz, E. C. *A Young Mind in a Growing Brain* (Lawrence Erlbaum, 2005).
5. Pujala, A. & Koyama, M. Chronology-based architecture of descending circuits that underlie the development of locomotor repertoire after birth. *eLife* **8**, e42135 (2019).
6. Hebb, D. O. *The Organization of Behavior: A Neuropsychological Theory* (John Wiley & Sons, 1949).
7. Hubel, D. H. & Wiesel, T. N. Brain mechanisms of vision. *Sci. Am.* **241**, 150–162 (1979).
8. Van Horn, M. R. & Ruthazer, E. S. Glial regulation of synapse maturation and stabilization in the developing nervous system. *Curr. Opin. Neurobiol.* **54**, 113–119 (2019).
9. White, J. G., Southgate, E., Thomson, J. N. & Brenner, S. The structure of the nervous system of the nematode *Caenorhabditis elegans*. *Phil. Trans. R. Soc. Lond. B* **314**, 1–340 (1986).
10. Scheffer, L. K. et al. A connectome and analysis of the adult *Drosophila* central brain. *eLife* **9**, e57443 (2020).
11. Karimi, A., Odenthal, J., Drawitsch, F., Boergens, K. M. & Helmstaedter, M. Cell-type specific innervation of cortical pyramidal cells at their apical dendrites. *eLife* **9**, e46876 (2020).
12. Morgan, J. L. & Lichtman, J. W. An individual interneuron participates in many kinds of inhibition and innervates much of the mouse visual thalamus. *Neuron* **106**, 468–481.e2 (2020).
13. Randel, N. et al. Inter-individual stereotypy of the *Platynereis* larval visual connectome. *eLife* **4**, e08069 (2015).
14. Kornfeld, J. et al. An anatomical substrate of credit assignment in reinforcement learning. Preprint at https://doi.org/10.1101/2020.02.18.954354 (2020).
15. Schneider-Mizell, C. M. et al. Chandelier cell anatomy and function reveal a variably distributed but common signal. preprint. Preprint at https://doi.org/10.1101/2020.03.31.018952 (2020).
16. Aicher, C., Jacobs, A. Z. & Clauset, A. Learning latent block structure in weighted networks. *J. Complex Netw.* **3**, 221–248 (2015).
17. Jin, X., Pokala, N. & Bargmann, C. I. Distinct circuits for the formation and retrieval of an imprinted olfactory memory. *Cell* **164**, 632–643 (2016).
18. White, J. G., Albertson, D. G. & Anness, M. A. Connectivity changes in a class of motoneurone during the development of a nematode. *Nature* **271**, 764–766 (1978).
19. Bargmann, C. I. & Marder, E. From the connectome to brain function. *Nat. Methods* **10**, 483–490 (2013).
20. Varshney, L. R., Chen, B. L., Paniagua, E., Hall, D. H. & Chklovskii, D. B. Structural properties of the *Caenorhabditis elegans* neuronal network. *PLoS Comput. Biol.* **7**, e1001066 (2011).

Methods

No statistical methods were used to predetermine sample size. The experiments were not randomized.

Electron microscopy

To learn emergent principles from studying synaptic changes of an entire brain across maturation, we analysed eight isogenic *C. elegans* beginning with the earliest larval stage and ending with the adult. Previous lineage studies revealed that the vast majority of post-embryonic neurogenesis and differentiation occurs during the L1 and L2 stages[21]. We reconstructed three L1, two L2 and one L3 worms at six different developmental time points, to afford the temporal resolution in capturing continuous connectomic changes during the period of most rapid growth. We reconstructed two adults to make direct comparisons between animals of the same age and with the original published connectome. While it took more than a decade to assemble the first *C. elegans* connectome[9], the advent of automation in sample sectioning, image acquisition and data processing sped up the process, enabling us to complete our brain reconstructions of multiple animals in less time.

We examined wild-type (Bristol N2) animals reared in standard conditions[21]: 35 × 10 mm NGM plates, fed by OP50 bacteria, and raised at 22.5 °C. The worms were within a few generations of the original stock acquired from *C. elegans* Genetics Center (CGC) in 2001. All samples used in this study were derived from three batches prepared for electron microscopy.

Each electron microscopy sample was prepared and processed as previously described[22] with small modifications to the substitution protocol of the last three datasets (protocol in preparation). In short, isogenic samples reared in the same environment were high-pressure frozen (Leica HPM100 for datasets 1–5 and Leica ICE for datasets 6–8) at different stages of post-embryonic development. High-pressure freezing was followed by freeze substitution in acetone containing 0.5% glutaraldehyde and 0.1% tannic acid, followed by 2% osmium tetroxide.

For each life stage, we selected samples on the basis of their overall size and morphology for electron microscopy analysis. The precise developmental age of each larva was determined after the electron microscopy reconstruction, by comparing its cellular compositions to stereotyped *C. elegans* cell lineage[23], as well as the extent of its neurite growth. Three samples (datasets 2, 6, and 7) were prepared for transmission electron microscopy (TEM). Five samples (datasets 1, 3, 4, 5 and 8) were prepared for scanning electron microscopy.

For TEM, samples were manually sectioned at ~50 nm using a Leica UC7 ultramicrotome, collected on formvar-coated slot grids (Electron Microscopy Sciences, FF205-Cu), poststained with 2% aqueous uranyl acetate and 0.1% Reynold's lead citrate, and coated with a thin layer of carbon. Images were manually acquired using an FEI Tecnai 20 TEM and a Gatan Orius SC100 CCD camera.

For scanning electron microscopy, samples were serial sectioned at ~30-40nm and collected using an automated tape-collecting ultramicrotome (ATUM)[24]. The tape was glued to silicon wafers, carbon coated, and sections post-stained with 0.5% uranyl acetate (Leica Ultrostain I, Leica Microsystems) and 3% lead citrate (Leica Ultrostain II, Leica Microsystems). Images were collected semi-automatically using custom software guiding an FEI Magellan XHR 400L[25].

All images were acquired at 0.64–2.00 nm per pixel (~25,000× magnification). In total, these datasets comprise 94,374 images, 5 teravoxels and 2.4×10^5 μm^3. Images were aligned using TrakEM2[26,27] and imported into CATMAID[28] for annotation.

Brain reconstruction

The brain was defined as the nerve ring and ventral ganglion, neuropil anterior of the ventral sub-lateral commissures. In every electron microscopy volume, all cells within the brain were manually reconstructed by skeleton tracing in CATMAID[28]. Neuron and muscle processes, but not glia processes, were also volumetrically segmented (Supplementary Table 4).

Every neuron, glia and muscle was annotated for chemical synapses to generate a connectome of the brain (Fig. 1b, Extended Data Fig. 2, Supplementary Video 2, Supplementary Table 2). Chemical synapse annotations include classical synapses, which contain mostly clear vesicles as well as a small number of dense core vesicles (DCVs), and synapses from modulatory neurons, which contains mostly DCVs (Extended Data Fig. 1a). Gap junctions were partially annotated and excluded from analyses. Chemical synapse weight was assessed by both the number and size of synapses. Each presynaptic active zone was volumetrically reconstructed to determine synapse sizes (Supplementary Table 3).

The same neurons were unambiguously identified in all datasets based on their soma position, neurite trajectory, and stereotypic morphological traits, as described[9]. In the original connectome datasets, as well as ours, some variability in cell body position and neurite trajectory was observed. However, every cell could still be unambiguously identified in every dataset because the combined anatomical features and neighbourhood for each cell is unique.

Negligible amounts of neuropil in our reconstructions could not be reliably traced to a known cell. These orphan fragments were small (median length 0.38 μm) and rare (4.13 ± 6.05 per dataset (mean ± s.d.)). Orphan fragments represent 0.18% of the total neurite length and 0.13% of all synapses and were excluded from analysis.

Synapse annotation

Chemical synapses and gap junctions were mapped manually. Chemical synapses were fully mapped and gap junctions were partially mapped. To reduce biases from different annotators, for chemical synapses, all datasets were annotated independently by three different people; only synapses that were agreed upon by at least two independent annotators were included in the final dataset.

Chemical synapse annotations include classical synapses, which contain mostly clear vesicles as well as a small number of DCVs, and synapses from modulatory neurons, which contains mostly DCVs (Extended Data Fig. 1a).

Modulatory neurons are distinguished from non-modulatory neurons by distinct features of their chemical synapses[29]. Classical synapses are made by all non-modulatory neurons; modulatory synapses are made by all modulatory neurons.

Classical synapses were identified by a characteristic presynaptic swelling containing a pool of clear vesicles adjacent to at least one dark presynaptic active zone on the inside of the membrane[22]. Each presynaptic active zone was annotated as the presynaptic partner of one chemical synapse. Cells adjacent to the active zone, within 100 nm in *xyz* dimensions, were identified as its potential postsynaptic partners. Synapse annotation included considerations for additional characteristics. Presynaptic swellings were also typically characterized by a small number of DCVs at the periphery of the active zone-associating and clear synaptic vesicle cloud, the presence of mitochondria, as well as the cadherin-like junctions between the pre- and postsynaptic partner cells[30]. Some postsynaptic partners exhibit morphological features such as swelling or postsynaptic densities (PSDs) that resemble the signature PSDs at the mammalian glutamatergic synapses.

Modulatory synapses appear as periodic varicosities along the modulatory neuron's neurite, each filled with a cloud of DCVs. Some modulatory synapses are devoid of clear synaptic vesicles; some have a small numbers of clear synaptic vesicles in these varicosities. Most DCV-specific varicosities do not have presynaptic active zones; the small amount of presynaptic active zones are often not associated with vesicles[29].

Gap junctions were partially annotated and not subjected to the consensus scoring process due to limitations of current sample preparation

methods[22]. They are shown at http://nemanode.org/ but were excluded from analyses due to incompleteness.

Volumetric reconstruction

For seven electron microscopy volumes, every neuron and muscle processes, but not glia processes, were volumetrically segmented (Supplementary Table 4). We computed the precise shape of every neurite and muscle process in each electron microscopy image based on the skeleton tracing that was performed in CATMAID and a machine learning algorithm that recognized cellular boundaries. Another algorithm expanded all skeleton nodes in each section until they fully filled the images of all labelled cell boundaries.

Cellular borders were predicted by a shallow Convolutional Neural Network (CNN) that builds on XNN[31,32], a recently developed high performance system that computes convolutions on CPUs, to achieve border prediction throughput[33,34] of ~10 MB/s. Node expansion was computed with a dedicated Cilk-based code[35] that parallelized the Dijkstra graph search algorithm. Code optimization allowed us to perform node expansion of an entire electron microscopy section in memory by a single multi-threaded process. Each software thread expanded an individual skeleton. Each pixel is attributed to a given cell by computing a generalized form of distance, taking into account the minimum number of cellular border pixels that must be traversed in a path connecting pixel and node. The generalized distance is computed using graph theory and concurrent data structures.

Volume traces were imported into VAST[36] for manual proofreading. At least 1,120 person-hours were spent proofreading the volumetric expansions. It was not possible to perform volumetric reconstruction on dataset 7 due to weak membrane contrast.

Spine-like protrusions

In parallel to neurite growth, there was extensive synapse addition. But only a small fraction of physical contacts developed into chemical synapses (Extended Data Fig. 1c). Presynaptic terminals appear as en passant boutons, most apposing the main neurite of a postsynaptic cell and some apposing small, spine-like protrusions[9,37].

These protrusions, short branches (<10% of the main neurite length), were found in many neurons and muscles (Extended Data Fig. 4f, g). From birth to adulthood, their number increased fivefold (Extended Data Fig. 4c), and the proportion apposing presynaptic terminals increased twofold (Extended Data Fig. 4d). In the adult connectome, small spine-like protrusions were postsynaptic at ~17% of total synapses (Extended Data Fig. 4a, b, Supplementary Table 5).

Protrusions apposing presynaptic termini were more likely to locate distally along a neurite, whereas protrusions not apposing presynaptic termini were more proximal (Extended Data Fig. 4e). Developmentally dynamic connections were twice as likely to involve spine-like protrusions than stable and variable connections (Extended Data Fig. 4h).

Cell-type classification

We followed conventional neuronal type classification[9], with modifications based on structural features revealed in this study and other studies.

Neurons were classified as motor neurons if they primarily made synapses onto muscles. Neurons were classified as sensory if they had specialized sensory processes and/or were previously reported to have sensory capabilities. Neurons were classified as interneurons if most of their connections were to other neurons. Neurons were classified as modulatory if they make chemical synapses that contained mostly large dark vesicles (DVCs) or if they had been reported to use serotonin (AIM, HSN), dopamine (ADE, CEP), or octopamine (RIC)[38,39]. Some neurons exhibit features corresponding to more than one type. In this case, they were classified based on their most prominent feature. A summary of the classification of each neuron and their justification is provided in Extended Data Fig. 10 and Supplementary Table 1.

Chemical synapse size

Presynaptic active zones were volumetrically reconstructed to determine synapse sizes in all electron microscopy volumes (Supplementary Table 3). Coordinates of all chemical synapses were exported from CATMAID[28] and imported into VAST[36] using custom scripts. The presynaptic active zone for every synapse was manually segmented throughout every section where it was visible. The size of monadic synapses is represented by the volume of the presynaptic active zone. At polyadic synapses, we estimated the relative strengths of postsynaptic partners by the proportion of postsynaptic area that each partner occupies at each synapse. We performed a Monte Carlo simulation of neurotransmitter diffusion from the presynaptic active zone, and quantified the proportion of these particles that reached each potential postsynaptic partner using the three-dimensional geometry of the electron microscopy reconstruction. Synapse size for each postsynaptic partner was calculated by multiplying the total volume of the presynaptic active zone by the proportion of particles that hit the membrane of each postsynaptic partner.

Connection classification

A total of 3,113 connections (averaging 1,292 per dataset) were assigned as stable, variable or developmentally dynamic as follows. A total of 1,647 connections (averaging 323 per dataset) had no more than two synapses in two or more datasets and were left–right asymmetric. These connections were classified as variable. The 1,466 remaining connections were pooled by left–right cell pairs, resulting in 658 pair connections. The number of synapses in each pair connection was tested for relative increase or decrease across maturation (Spearman's rank correlation, corrected for multiple comparisons using the Benjamini–Hochberg correction). Pair connections showing a significant change and at least a fivefold change in synapse number from birth to adulthood were classified as developmentally dynamic. When a connection is absent from dataset 1 and 2, but exists in later datasets, we consider it to have increased more than fivefold (an 'infinite' increase). Remaining pair connections were considered stable if they were present in at least seven datasets, and variable if present in fewer than seven datasets. The fivefold change cut-off is based on the overall expansion in synapse number from early L1 to adulthood. Occasionally, connections were near the cut-off for developmentally dynamic versus variable connections. How they are categorized does not affect any overall pattern in our connectome analysis due to the extremely small number.

Prevalence and validation of variable connections

When comparing connectomes from individuals at different developmental stages, we found a surprisingly substantial proportion of synapses and connections to be variable from animal to animal. Moreover, not all variable connections consisted of few synapses and not all stable connections consisted of many synapses (Extended Data Fig. 6g, h). The range of synaptic strength for both stable and variable connections makes it difficult to set them apart by thresholding: any threshold to filter postsynaptic partners—by synapse number, synapse size, or number of postsynaptic partners—excluded both variable and stable connections (Extended Data Fig. 6g, h).

We assessed the possibility that variability is more prominent during development than in the mature connectome. A conservative measure of variability in the adult stage can be made by comparing our two adult datasets and the original adult connectome[9]. When using these adult datasets to quantify variability, variable connections still made up ~50% of all connections (Extended Data Fig. 9a, b). Thus, variable connections are prominent in the *C. elegans* connectome across development.

The higher prevalence of variable connections between certain cell types remained evident when variable connections were defined only among adult datasets (Extended Data Fig. 9c) and when connections with fewer synapses were excluded (Extended Data Fig. 6h). The low

variability of connections from motor neurons to muscles could not be explained simply by saturation of their physical contacts by synapses (Extended Data Fig. 9d). We also considered that neurons with more synapses may exhibit more stochastic synapses or have more annotation errors. However, the proportion of variable connections did not scale with the number of synapses (Extended Data Fig. 9e, f).

The developmental age of each dataset

The developmental age of each sample was established based on the described temporal cell division pattern exhibited by wild-type (N2) larva raised[23] at 25 °C.

Dataset 1: L1 at birth. No Q cell division, which occurs ~3 h post-hatching (after birth). Q cell nuclei are symmetrical, before nuclei migration, which occurs ~2 h after birth, placing this sample so close to birth, estimated to be ~0 h.

Dataset 2: L1 estimated to be 5 h. Q cell divided but no H1 division, which occurs at~7.5 h after birth. We found that PVC neurites were partially grown out and SAA posterior neurites had not begun to grow at this time point, indicating an age slightly more than halfway between datasets 1 and 3.

Dataset 3: L1 at 8 h. With H1 just completing its division and P5/6 starting their migration, this sample was placed at ~8 h after birth, when both events take place.

Data set 4: L1 at the very end of the larval stage, near the end of the L1 lethargus. It is estimated to be 16 h. It has two layers of cuticle. Both P11.aaa and P12.aaa have divided. V5R.p is in the midst of division, and H1.a has not yet divided; all happen at ~16 h after birth.

Dataset 5: L2 towards the end of the larval stage (23 h). SML/R have not divided, which occurs at ~29 h. It has 40 gonad cells, and a slight double cuticle that indicates the end of L2. However, its gut lumen contains food, placing this sample shortly before entering L2 lethargus, which occurs at ~23 h.

Dataset 6: L3 at 27 h. Based on the partial outgrowth of the RMF neurites, which is born at 23 h, this sample was estimated to be ~27 h.

Datasets 7 and 8: Young adults at 45 h. Both samples have adult cuticles but are relatively small compared to other adults. The exact ages of the two young adult samples are uncertain, so they are treated as equals for analyses.

Anatomical inconsistencies between samples

Similar to observations of the original studies[9], a few anatomic inconsistencies are observed in some datasets, likely due to heterogeneity or imprecision of development processes. These events do not have an impact on overall connectivity, as all non-variable connections between individual neuron classes were conserved. Neurons in these datasets did not exhibit more variable connections either.

Dataset 2: CEPDL cell body is shifted to the anterior ganglion.

Dataset 3: RIFL neurite terminates prematurely laterally, not reaching the dorsal midline.

Dataset 4: RIH cell body is shifted to the anterior ganglion. PVCL and PVCR neurites both go right-handedly around the nerve ring, appearing as PVCR.

Dataset 5: RMHL and RMHR neurites both traverse right-handedly around the nerve ring, appearing as RMHR. ADAL terminates prematurely at a dorsal sub-lateral position, not reaching the dorsal midline.

Dataset 6: PVR neurite is fragmented.

Dataset 7: RIFL and RIFR neurites both traverse right-handedly around the nerve ring, appearing as RIFR.

Comparison to the original *C. elegans* adult connectome

The original adult hermaphrodite brain connectome annotated by White et al.[9,40] was taken from *wormatlas.org* (dataset N2U). Because individual muscles were not traced in the original annotation, we completed this dataset by tracing through all head muscles using the scanned electron microscopy micrographs hosted by http://wormatlas.org. Individual muscles arms were identified by their characteristic location within the brain, which were confirmed by tracing the arms back to their cell body in several datasets. This augmented dataset (referred to as 'N2U, White et al., 1986') was used for subsequent comparison.

The wormatlas.org site hosts a re-annotated version of the wiring of the N2U connectome, which includes synapses to individual muscles from ref. [41]. We noted errors in muscle identification and synapse annotation in this reannotation. We corrected some errors so that we could perform comparisons with our analysis. Specifically, we corrected the identity of the following muscle pairs VL1–VL2, VR1–VR2, DL2–DL3, DR2–DR3, DL5–DL6, DR5–DR6, VL5–VL6 and VR5–VR6. Other mistakes in tracing and synapse annotation could not be corrected. For example, muscles DL7 and DL8 were not traced at all in the brain, and only one of more than 50 synapses onto muscle VR2 (named as VR1 in ref. [41]) was annotated. This minimally corrected dataset, referred to as 'N2U, Cook et al., 2019' was used for subsequent comparison.

For both N2U datasets, we only included neurons and neurites within the same regions used for our datasets for comparison.

Community structure analysis

Weighted stochastic block modelling (WSBM)[16] was used to define modules individually for all eight connectomes. In this approach, modules are optimized on the likelihood of observing the actual network from the determined modules (log-likelihood score) based on two exponential family distributions. We chose the probability of establishing connections to follow a Bernoulli distribution and the synapse number for each connection to follow an exponential distribution. These distributions fit the data best according to the log-likelihood score and resulted in left–right cell pairs being assigned to the same modules.

In order to find a stable and representative number of modules for each connectome, we used a consensus-based model-fitting approach, similar to the one described previously[42]. First, to ensure unbiased coverage of the parameter space, we fitted the model independently 300 times using an uninformative prior for each potential number of modules ($k = 1, \ldots, 8$). This procedure was repeated 100 times to yield a collection of models with concentrated and unimodally distributed log evidence scores. To improve the stability of the models on multiple runs, we increased the parameters for a maximum number of internal iterations to 100. For each dataset, we chose the number of modules whose collection of models had the highest mean posterior log-likelihood score. For dataset 2 the second-highest score was selected, as the number of modules otherwise conflicted with adjacent time points.

Finally, for each dataset, we found a representative consensus module assignment that summarized all 100 models[42]. In brief, considering all 100 models, we calculated the frequency of each cell being assigned to each module, and used this as a new before fit another 100 models. This procedure was repeated until convergence, when the consistency of the 100 models was larger than 0.95.

Data processing for analysis

To calculate the contact area of each adjacent cell pair, volumetric neuron and muscle traces were exported from VAST[17] and imported into MATLAB. Electron microscopy artefacts were manually corrected. We performed two-dimensional morphological dilation of every traced segment across extracellular space until neighbouring segments made contact within 70 pixels (140–280 nm). Expansion was restricted to the edge of the nerve ring. The total contact area was calculated as the sum of adjacent pixels for each segment in all sections. Contacts between cell bodies at the periphery of the neuropil were excluded.

To analyses related to neurites, synapses and connections, neuron skeletons and synapses were exported from CATMAID using custom Python scripts, and imported into Python or MATLAB environments for analyses. The module detection analysis was performed in MATLAB. Other analyses were implemented with custom Python scripts using

SciPy and Statsmodels libraries for statistics. Post-embryonically born neurons were excluded from analyses related to classification of connections, feedforward information flow, and modules.

For analyses related to neurites, both processes of neurons and muscles in the nerve ring were included. The length was calculated using the smoothened skeleton of each neurite. The skeleton was smoothed by a moving average of 10 skeleton nodes after correction of major alignment shifts. Spine-like protrusions were defined as any branch shorter than 10% of the average neuron length.

For analyses related to information flow, analyses for feedforward, feedback, and recurrent connections excluded connections to muscles since they are all feedforward.

Statistics

Statistical methods were not used to predetermine sample sizes. Spearman's rank was used for all correlations (Fig. 1j, Extended Data Figs. 1c, g, h–j, 9e, f) and time series (Extended Data Figs. 1l, 2a–c, 3b, 4b–d). Two-tailed *z*-test was used to compare proportions (Fig. 2e, Extended Data Fig. 7c). To determine if developmentally dynamic connections were over- or underrepresented, the proportions of developmentally dynamic connections between each cell type were compared to the total proportion of developmentally dynamic connections throughout all cell types (Fig. 2e, Extended Data Fig. 4h). Kruskal–Wallis test followed by pairwise Mann–Whitney *U* tests were used for comparisons of more than two unpaired categories (Extended Data Figs. 1k, 4h, 6j, 9c, 7b). For figure panels with more than three categories, only categories statistically different from all others were labelled (Extended Data Figs. 4h, 6j, 9c). For figure panels with multiple comparisons, the reported *P*-values were FDR-adjusted using Benjamini–Hochberg correction.

Limitations

We have not included gap junctions, critical components of the nervous system, in our analysis. Our online connectome database (http://nemanode.org/) includes electrical synapses where gap junctions were most visible. But improvements in sample preparation and analysis are needed to reach the same level of confidence and throughput as we reached for chemical synaptic networks throughout development.

We have analysed only one connectome at most time points. This enabled us to compare stable, variable and developmentally dynamic synaptic networks across development but not to assess animal-to-animal variability at each age. Increased throughput and the analysis of many animals at each age will allow analysis of the statistical properties of synaptic connectivity.

Reporting summary

Further information on research design is available in the Nature Research Reporting Summary linked to this paper.

Data availability

All electron microscopy images and volumetric reconstructions are available at https://bossdb.org/project/witvliet2020. Connectivity matrices for all datasets are available at http://www.nemanode.org and as Supplementary Tables.

Code availability

All scripts and files used to generate all figures are available at https://github.com/dwitvliet/nature2021.

21. Brenner, S. The genetics of *Caenorhabditis elegans*. *Genetics* **77**, 71–94 (1974).
22. Mulcahy, B. et al. A pipeline for volume electron microscopy of the *Caenorhabditis elegans* nervous system. *Front. Neural Circuits* **12**, 94 (2018).
23. Sulston, J. E. & Horvitz, H. R. Post-embryonic cell lineages of the nematode, *Caenorhabditis elegans*. *Dev. Biol.* **56**, 110–156 (1977).
24. Baena, V., Schalek, R. L., Lichtman, J. W. & Terasaki, M. Serial-section electron microscopy using automated tape-collecting ultramicrotome (ATUM). *Methods Cell Biol.* **152**, 41–67 (2019).
25. Hayworth, K. J. et al. Imaging ATUM ultrathin section libraries with WaferMapper: a multi-scale approach to EM reconstruction of neural circuits. *Front. Neural Circuits* **8**, 68 (2014).
26. Cardona, A. et al. TrakEM2 software for neural circuit reconstruction. *PLoS One* **7**, e38011 (2012).
27. Saalfeld, S., Fetter, R., Cardona, A. & Tomancak, P. Elastic volume reconstruction from series of ultra-thin microscopy sections. *Nat. Methods* **9**, 717–720 (2012).
28. Saalfeld, S., Cardona, A., Hartenstein, V. & Tomancak, P. CATMAID: collaborative annotation toolkit for massive amounts of image data. *Bioinformatics* **25**, 1984–1986 (2009).
29. Lim, M. A. et al. Neuroendocrine modulation sustains the *C. elegans* forward motor state. *eLife* **5**, e19887 (2016).
30. Hung, W. L. et al. Attenuation of insulin signalling contributes to FSN-1-mediated regulation of synapse development. *EMBO J.* **32**, 1745–1760 (2013).
31. Kasthuri, N. et al. Saturated reconstruction of a volume of neocortex. *Cell* **162**, 648–661 (2015).
32. Meirovitch, Y. et al. A multi-pass approach to large-scale connectomics. Preprint at https://arxiv.org/abs/1612.02120 (2016).
33. Matveev, A. et al. A multicore path to connectomics-on-demand. In *Proc. 22nd ACM SIGPLAN Symposium on Principles and Practice of Parallel Programming*, 267–281 (2017).
34. Meirovitch, Y. et al. Cross-classification clustering: an efficient multi-object tracking technique for 3-d instance segmentation in connectomics. In *Proc. IEEE Conference on Computer Vision and Pattern Recognition*, 8425–8435 (2019).
35. Blumofe, R. D. et al. Cilk: An efficient multithreaded runtime system. *J. Parallel Distrib. Comput.* **37**, 55–69 (1996).
36. Berger, D. R., Seung, H. S. & Lichtman, J. W. VAST (volume annotation and segmentation tool): efficient manual and semi-automatic labeling of large 3D image stacks. *Front. Neural Circuits* **12**, 88 (2018).
37. Philbrook, A. et al. Neurexin directs partner-specific synaptic connectivity in *C. elegans*. *eLife* **7**, e35692 (2018).
38. Sulston, J., Dew, M. & Brenner, S. Dopaminergic neurons in the nematode Caenorhabditis elegans. *J. Comp. Neurol.* **163**, 215–226 (1975).
39. Duerr, J. S. et al. The *cat-1* gene of *Caenorhabditis elegans* encodes a vesicular monoamine transporter required for specific monoamine-dependent behaviors. *J. Neurosci.* **19**, 72–84 (1999).
40. Durbin, R. M. *Studies on the Development and Organisation of the Nervous System of Caenorhabditis elegans* (Univ. of Cambridge, 1987).
41. Cook, S. J. et al. Whole-animal connectomes of both *Caenorhabditis elegans* sexes. *Nature* **571**, 63–71 (2019).
42. Faskowitz, J., Yan, X., Zuo, X.-N. & Sporns, O. Weighted stochastic block models of the human connectome across the life span. *Sci. Rep.* **8**, 12997 (2018).

Acknowledgements We thank V. Laskova for help with electron microscopy samples; B. Harris for help with high-pressure freezing; M. Neubauer, D. Kersen, A. Paulino, M. Suriyalaksh, A. Srajer, M. Chang, S. Ihn and J. Ho for help with imaging; A. Cardona, I. Arganda-Carreras and J. Qian for guidance on electron microscopy alignment; S. Cook, C. Rehaluk and M. Wang for synapse annotation in some datasets; J. Ho, C. Morii-Sciolla, I. So, M. and C.-Y. Ho for generating ground truth and proofreading for volumetric reconstruction; A. Matveev, L. Mi and H. Saribekyan for help with analysis algorithms; J. Wang and D. Cao for help with statistics; A. Lin, C. Tabone and V. Venkatachalam for help with data servers; S. Maeng and D. Fong for help with www.nemanode.org; members of our laboratories for comments; G. Si and L. Varshney for critical reading and suggestions; D. Hall, J. Srinivasan and A. Cardona for early advice. J.K.M. was supported by NSF PoLS (NSF 1806818). B.M. was supported by the Mount Sinai Foundation. J.W.L. was supported by the NIMH, Silvio Conte Center (P50 MH094271), the NIH (U24 NS109102-01) and MURI (GG0008784). J.W.L., A.D.T.S. and M.Z. were supported by the HFSP (RGP0051/2014). A.D.T.S. and M.Z. were supported by the NIH (R01-NS082525-01A1). A.D.T.S. was supported by NIH Brain Initiative (1U01NS111697-01) and NSF BRAIN EAGER (IOS-1452593). M.Z. was supported by CIHR (MOP-123250 and Foundation Scheme 154274), the Radcliffe Institute and the Mount Sinai Foundation.

Author contributions J.W.L., A.D.T.S. and M.Z. conceived the study. Y.M., R.P. and N.S. designed the algorithm for automated volumetric reconstruction (contact Y.M. at yaron.mr@gmail.com). D.R.B. and R.L.S. designed the pipeline for automated electron microscopy acquisition (contact D.R.B. at danielberger@fas.harvard.edu). Y.W. designed software for electron microscopy alignment (contact Y.W. at yuelongwu@fas.harvard.edu). D.W., B.M., J.K.M., D.H., R.L.S. and M.Z. generated and imaged most of the electron micrographs. D.W., B.M. and J.K.M. performed most annotation. D.W. designed and performed most analysis. D.R.B., W.X.K. and Y.L. performed additional experiments and analysis. A.D.C. guided early cell identification and annotation. D.W., J.W.L., A.D.T.S. and M.Z. wrote the manuscript. All authors reviewed the manuscript.

Competing interests The authors declare no competing interests.

Additional information

Supplementary information The online version contains supplementary material available at https://doi.org/10.1038/s41586-021-03778-8.

Correspondence and requests for materials should be addressed to D.W., J.W.L., A.D.T.S. or M.Z.

Peer review information *Nature* thanks the anonymous reviewer(s) for their contribution to the peer review of this work. Peer reviewer reports are available.

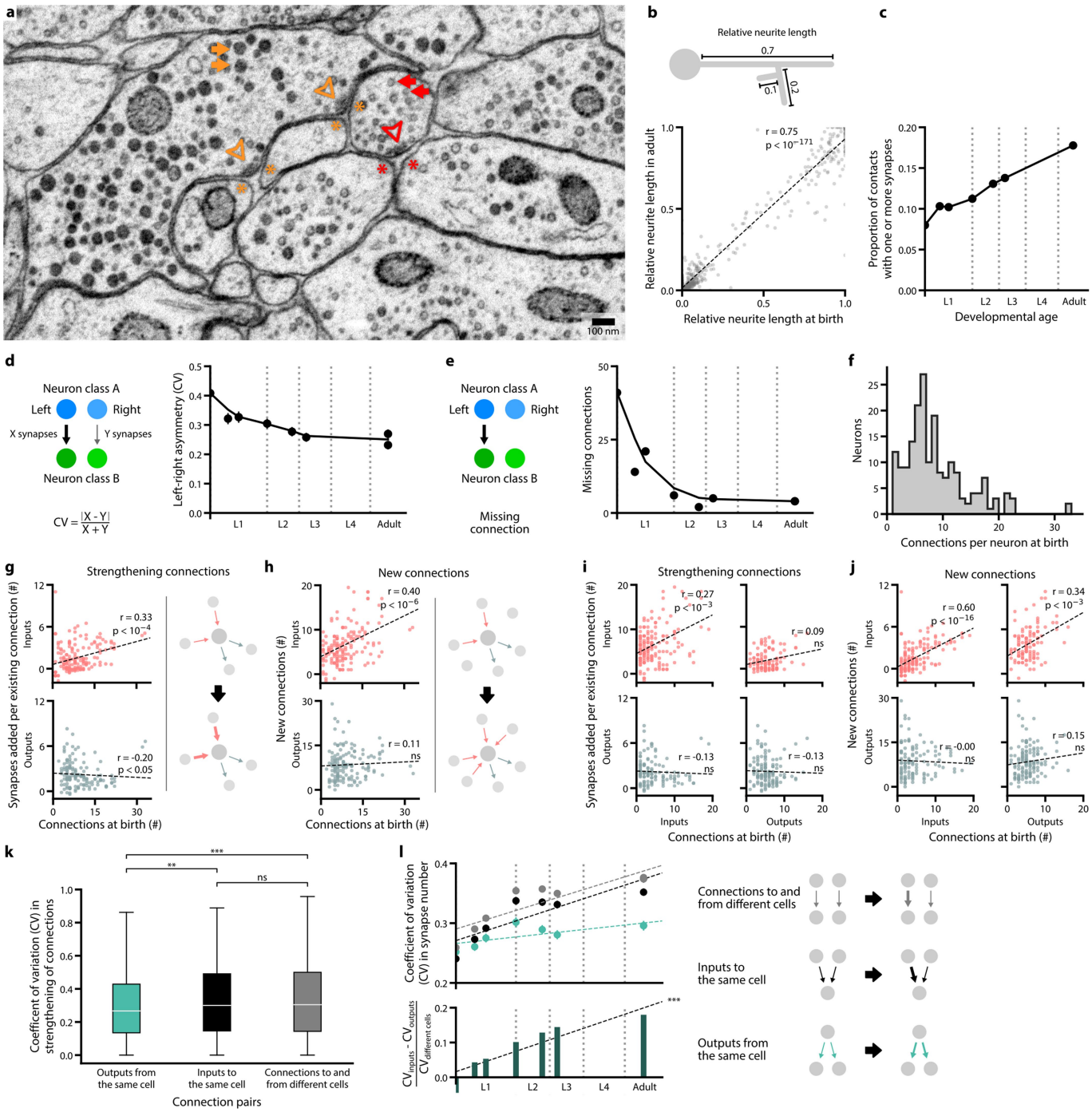

Extended Data Fig. 1 | See next page for caption.

Extended Data Fig. 1 | Electron microscopy reconstruction of cells and synapses in *C. elegans* brains from birth to adulthood. a, A representative electron microscopy micrograph of the neuropil (from dataset 3). Presynaptic termini of classical chemical synapses are characterized by a pool of clear synaptic vesicles (red arrows) surrounding an active zone (red arrowhead). Presynaptic termini of chemical synapses of modulatory neurons are characterized by mostly DCVs (orange arrows) distant from the active zone (orange arrowhead). Postsynaptic cells are marked by asterisks. The proportion of dense core and clear synaptic vesicles were not quantified. **b**, Neurites grow while maintaining overall brain geometry. Correlation of the relative neurite length of each branch between L1 (dataset 1) and adult (dataset 8). The length of each neurite is normalized against the total neurite length of the neuron. $P = 9.4 \times 10^{-172}$, $r = 0.75$, $n = 947$, Spearman's rank correlation. **c**, Proportion of physical contacts in the brain that harbours at least one chemical synapse at respective developmental time points. **d**, Most connectivity asymmetry at birth is eliminated during L1. Connectivity asymmetry decreases from birth to adulthood, most significantly during L1. Asymmetry is defined as the coefficient of variation (CV) in synapse number between left-right cell pairs. Error bars indicate s.e.m. **e**, Total number of missing connections decreases from birth to adulthood, most significantly during L1. One connection refers to a cell making at least one chemical synapse to another cell. A missing connection is defined as a connection absent in only one dataset and from one side of the brain. **f**, Non-uniform distribution of connections and strengthening of connections across maturation. Distribution of the total number of input and output connections per neuron at birth. **g**, Non-uniform synapse addition to synaptic inputs and outputs of a cell. Top: neurons with higher number of connections at birth (dataset 1) are more likely to receive new synapses at existing input connections by adulthood (averaging datasets 7 and 8). Bottom: no correlation is observed at existing output connections. Each data point represents one cell. Significance is calculated using two-sided Spearman's rank correlation (top: $P = 1.1 \times 10^{-5}$, $n = 166$; bottom: $P = 0.017$, $n = 141$). **h**, Top: neurons with higher number of connections at birth (dataset 1) are more likely to establish new input connections by adulthood (averaging datasets 7 and 8). Bottom: no correlation is observed at new output connections. Each data point represents one cell. Significance is calculated using two-sided Spearman's rank correlation (top: $P = 1.3 \times 10^{-7}$, $n = 166$; bottom: $P = 0.18$, $n = 141$). **i**, Upper panels: neurons with more input connections at birth are more likely to strengthen these connections during maturation. Left: the number of input connections at birth (dataset 1) is positively correlated with their synapse number increase by adulthood (average of datasets 7 and 8). $P = 1.6 \times 10^{-17}$, $n = 166$ by the Spearman's rank correlation. Right: the number of output connections at birth does not predict the synapse number increase at input connections by adulthood. $P = 0.32$, $n = 120$ by the Spearman's rank correlation. Lower panels: Neither input connection (left) nor output connection (right) at birth predicts the synapse number increase at output connections by adulthood. left: $P = 0.16$, $n = 120$; right: $P = 0.12$, $n = 141$ by the two-sided Spearman's rank correlation. Each point represents one cell. **j**, Upper panels: neurons with higher number of input connections (left) or output connections (right) at birth (dataset 1) are more likely to establish new input connections by adulthood (average of datasets 7 and 8). Left: $P = 5.4 \times 10^{-4}$, $n = 166$; right: $P = 1.7 \times 10^{-4}$, $n = 120$ by the Spearman's rank correlation. Lower panels: Neither the input (left) or output (right) connection number at birth predicts the likelihood to establish new output connections by adulthood. Left: $P = 1.00$, $n = 120$; right: $P = 0.08$, $n = 141$ by the two-sided Spearman's rank correlation. Each data point represents one cell. **k**, Relative number of synapses added to existing connections is correlated between outputs of the same cell compared to connections to and from different cells. Relative number of synapses added represents the fold increase of synapse number from birth (dataset 1) to adulthood (average of datasets 7 and 8). ns (not significant) $P = 0.48$, $^{**}P = 4.5 \times 10^{-3}$, $^{***}P = 4.9 \times 10^{-5}$, two-sided Mann–Whitney *U* test, FDR adjusted using Benjamini–Hochberg correction ($n_{outputs} = 753$, $n_{inputs} = 1203$, $n_{other} = 90709$). Centre line, median; box limits, upper and lower quartiles; whiskers, 1.5x interquartile range; outliers not shown. Top: each data point represents the mean coefficient of variation (CV) in the number of synapses for different sets of connections. The CV of output connections from the same cell is maintained. The CV of input connections to the same cell increases over time, at the same rate as connections to and from different cells. Error bars indicate s.e.m. Bottom: the difference between the mean CV for output and input connections relative to connections between different cells grows over time. $^{***}P = 5.3 \times 10^{-7}$, $r = 0.99$, two-sided Spearman's rank correlation.

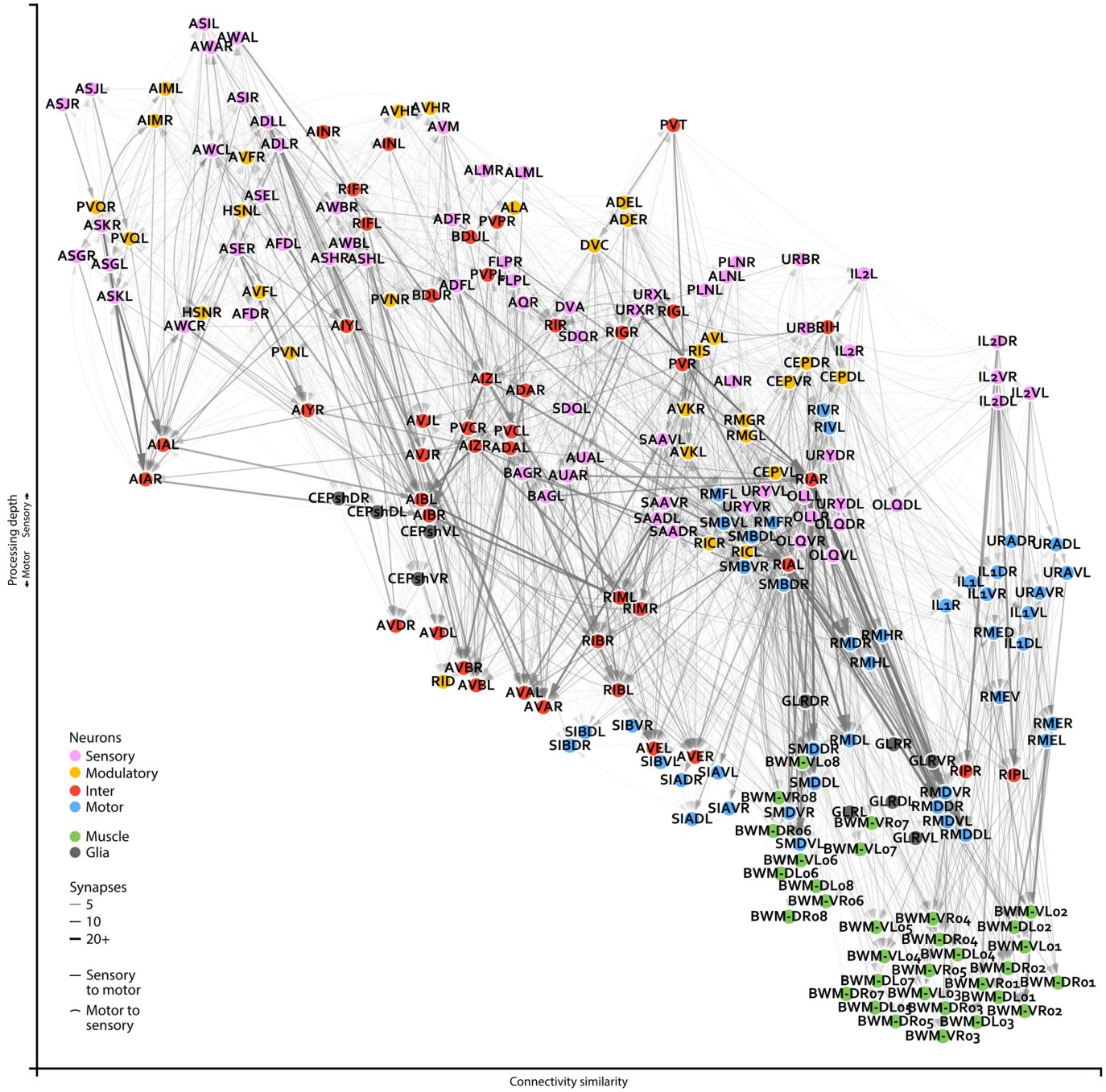

Extended Data Fig. 2 | Closeup of an adult brain connectome. Wiring diagrams for an adult connectome (dataset 8). Each circle represents a cell. Circle colour denotes cell type. Each line represents a connection with at least one chemical synapse between two cells. Line width indicates synapse number. Straight lines direct information from sensory to muscle layers whereas curved lines direct information in reverse. Cell coordinates are represented as in Fig. 1b, with overlapping cells manually separated.

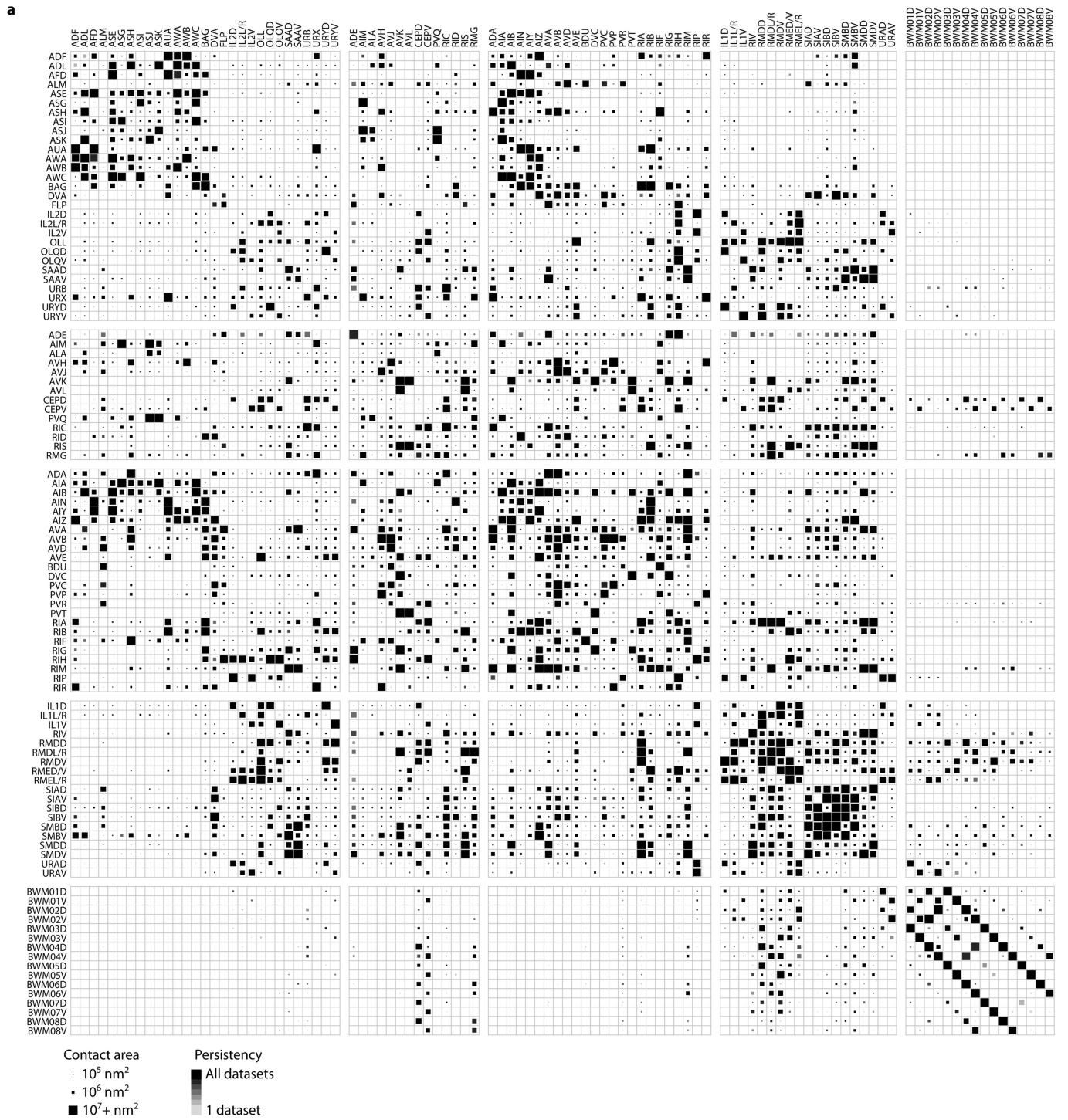

Extended Data Fig. 3 | A physical contact matrix between neurites and muscle fibres in seven volumetrically reconstructed *C. elegans* brains. Cells are pooled by left-right pairs. The physical contact size is represented by the largest value from the seven datasets. Statistical significance calculated by two-sided Spearman's rank correlation.

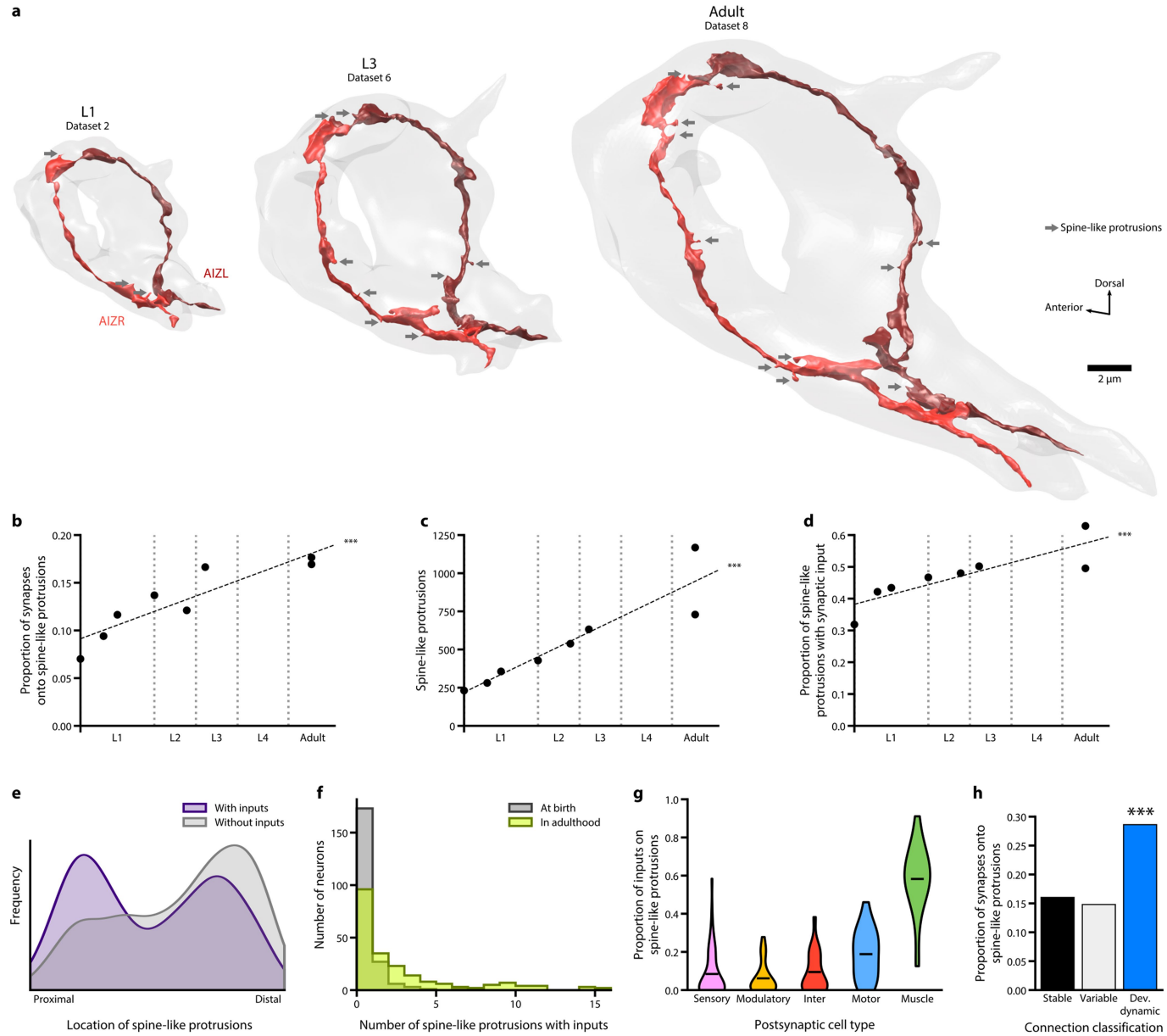

Extended Data Fig. 4 | Prevalence, location, and synaptic distribution of spine-like protrusions. a, 3D reconstructions of one neuron class (AIZL and AIZR) across maturation. The overall geometry was maintained, whereas the number of spine-like protrusions (grey arrows) increased over time. **b**, Proportion of postsynaptic spine-like protrusions increases across maturation. *** $P = 6.5 \times 10^{-5}$, two-sided Spearman's rank correlation. **c**, Total number of spine-like protrusions in the brain increases across maturation. *** $P = 5.3 \times 10^{-7}$, two-sided Spearman's rank correlation. **d**, Proportion of synapses with at least one spine-like protrusion postsynaptic partner increases across maturation. *** $P = 1.8 \times 10^{-4}$, two-sided Spearman's rank correlation. **e**, Distribution of spine-like protrusions by location, with the entry of the neurite into the brain as the most proximal, and the exit or terminal end of the neurite the most distal. **f**, Number of spine-like protrusions that oppose a presynaptic terminal per neuron at birth (average of datasets 1 and 2) and in adulthood (average of datasets 7 and 8). **g**, Proportion of presynaptic inputs onto spine-like protrusions per neuron in adulthood (average of datasets 7 and 8), grouped by their cell type. **h**, Proportion of synapses with spine-like protrusions that comprise stable, variable, and developmentally dynamic connections. Developmentally dynamic connections have the highest proportion. *** (stable-dev. dynamic) $P = 3.7 \times 10^{-34}$, *** (variable-dev. dynamic) $P = 5.1 \times 10^{-25}$, two-tailed Z-test, FDR adjusted using Benjamini–Hochberg correction ($n_{stable} = 10{,}059$, $n_{variable} = 2{,}169$, $n_{dev.dynamic} = 1{,}611$).

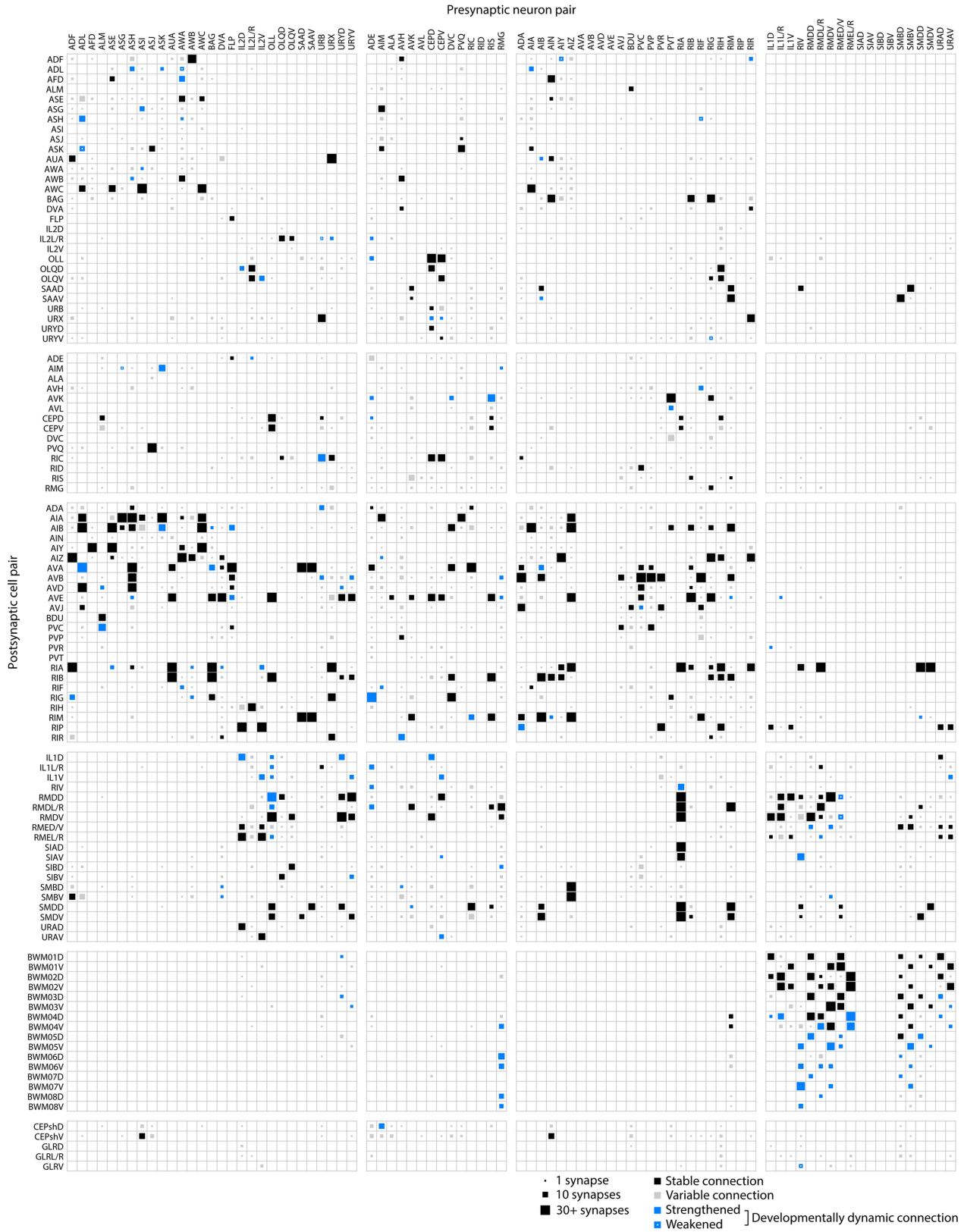

Extended Data Fig. 5 | Connectivity matrix of the *C. elegans* brain throughout maturation. Connectivity matrix including connections observed in eight *C. elegans* brains. Cells are pooled by left-right pairs. Each connection size represents the largest synapse number in any dataset. Stable, developmentally dynamic, and variable connections are colour-coded (Methods).

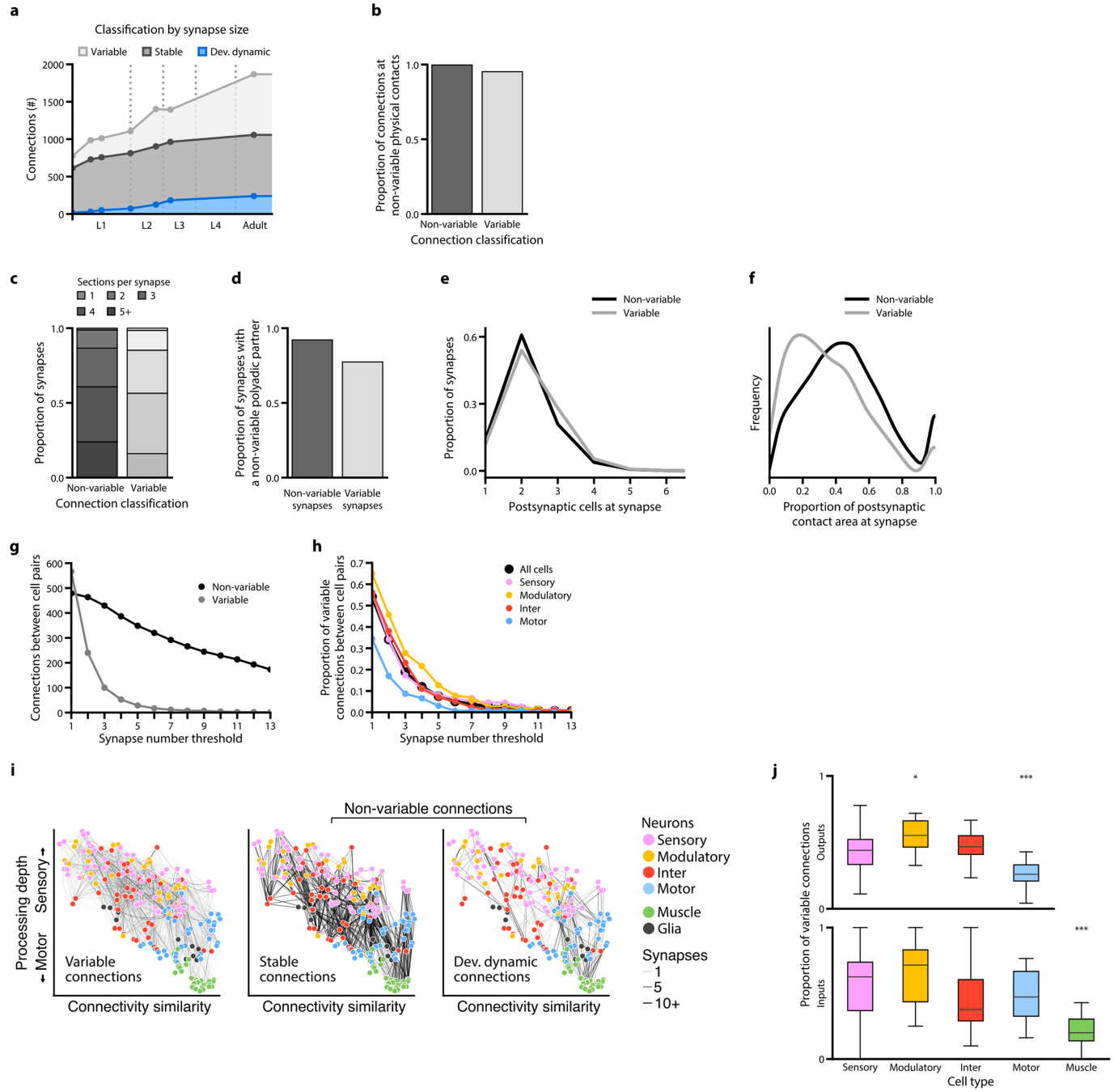

Extended Data Fig. 6 | See next page for caption.

Extended Data Fig. 6 | A connectome has prevalent variable connections. **a**, Composition of stable, developmentally dynamic, and variable connections in each dataset classified by synapse size. **b**, Prevalence of variable connections is not caused by over-annotation of ambiguous synapses. High proportions of both variable and non-variable (stable and developmentally dynamic) connections form at non-variable physical contacts. A physical contact is defined as variable when it is absent from more than one of the seven datasets. **c**, Synapses that constitute non-variable and variable connections, sorted by electron microscopy section numbers that the presynaptic active zone encompasses. All synapses in seven volumetrically segmented datasets are included. Synapses comprising variable connections are marginally smaller that those comprising non-variable connections, but no threshold can be set to remove exclusively the variable connections. **d**, Proportion of synapses that form a polyadic synapse with synapses of the stable connections. A marginally smaller portion of synapses that comprise variable connections (78%) than those comprising non-variable connections (93%) reside in this configuration. Therefore, variable connections are not fortuitous accidents of synapse annotation. **e**, Synapses comprising non-variable and variable connections sorted by the number of post-synaptic partners. They exhibit similar distributions from monoadic to polyadic. Non-variable connections have marginally more polyadic synapses than variable connections (20% vs 28% for dyadic, and 61% vs 54% for triadic synapses, respectively). No threshold by postsynaptic partner number can be set to filter variable connections. **f**, Proportion of postsynaptic contact area occupied by each postsynaptic partner at each synapse. Synapses comprising variable connections on average occupy less postsynaptic area than synapses comprising non-variable connections, but no threshold can be set to only exclude variable connections. **g**, Any threshold removes both variable and non-variable connections. Total number of non-variable (stable and developmentally dynamic) and variable connections in adulthood (average of datasets 7 and 8) upon thresholding by different synapse numbers. No synapse number provides a filter for specific removal of variable connections: all removes both variable and stable connections. **h**, Thresholding connections by synapse number leaves substantial proportion of variable connections for all cell types. Non-uniform distribution of variable connections remains when connections with low synapse numbers are removed. **i**, Non-uniform distribution of variable and developmentally dynamic connections. Wiring diagrams for variable, stable, and developmentally dynamic connections. Each line represents a connection observed in at least one dataset. Line width indicates the largest number of synapses observed for a connection across datasets. Each circle represents a cell. Cell coordinates are represented as in Fig. 1b. Comparison of the proportion of variable and non-variable connections for each cell type. Non-variable connections include stable and developmentally changing connections. Cell types with significantly higher or lower proportions of variable connections are indicated. Upper panel: $*P$ (modulatory-inter) = 2.2×10^{-2}, $*P$ (modulatory-sensory) = 6.5×10^{-3}, $***P$ (sensory-motor) = 4.7×10^{-8}, $***P$ (modulatory-motor) = 5.2×10^{-8}, $***P$ (inter-motor) = 1.7×10^{-7}, lower panel: $***P$ (sensory-muscle) = 6.9×10^{-9}, $***P$ (modulatory-muscle) = 1.3×10^{-7}, $***P$ (inter-muscle) = 3.6×10^{-5}, $***P$ (motor-muscle) = 8.1×10^{-7}. n = 22-57, two-sided Mann–Whitney U test, FDR adjusted using Benjamini–Hochberg correction. Centre line, median; box limits, upper and lower quartiles; whiskers, 1.5x interquartile range; outliers not shown.

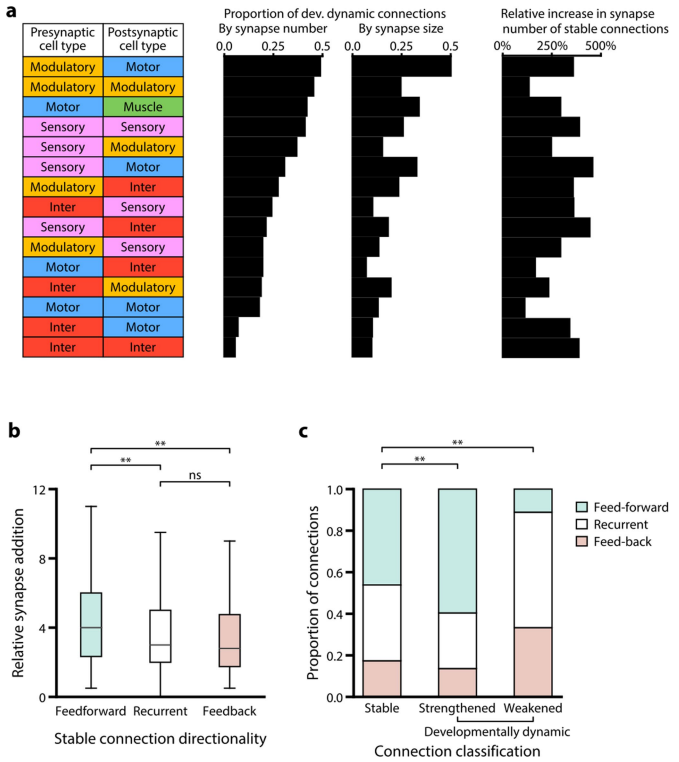

Extended Data Fig. 7 | Stability of interneuron connections and strengthening of feedforward connections are revealed by assessing connection strength by synapse size. a, Proportion of developmentally dynamic connections by cell type, when connection strength changes were evaluated by either synapse number (left) or synapse size (middle). Connections between interneurons are the most stable regardless of how synapse weight was evaluated. Right panel: Developmental stability of connections is not correlated with the extend of synapse number increase from birth (average of datasets 1 and 2) to adulthood (average of datasets 7 and 8). **b**, Increase in both feedforward signal flow and modularity across maturation. The number of synapses for stable connections in adults (datasets 7 and 8) relative to birth (datasets 1 and 2). Stable feedforward connections are strengthened more than stable feedback and recurrent connections. ns (not significant) $P = 0.13$, $^{**}P$ (feedforward-recurrent) = 0.0015, $^{**}P$ (feedforward-feedback) = 0.0012, two-sided Mann–Whitney U test, FDR adjusted using Benjamini–Hochberg correction ($n_{feedforward} = 301$, $n_{recurrent} = 229$, $n_{feedback} = 107$). Centre line, median; box limits, upper and lower quartiles; whiskers, 1.5x interquartile range; outliers not shown. **c**, Proportions of feedforward, feedback, and recurrent connections for stable and developmentally dynamic connections. $^{**}P$ (stable-strenghened) = 0.0015, $^{**}P$ (stable-weakened) = 0.0032, two-tailed Z-test of the proportion of feedforward connections, FDR adjusted using Benjamini–Hochberg correction ($n_{stable} = 737$, $n_{added} = 198$, $n_{weakened} = 18$).

a

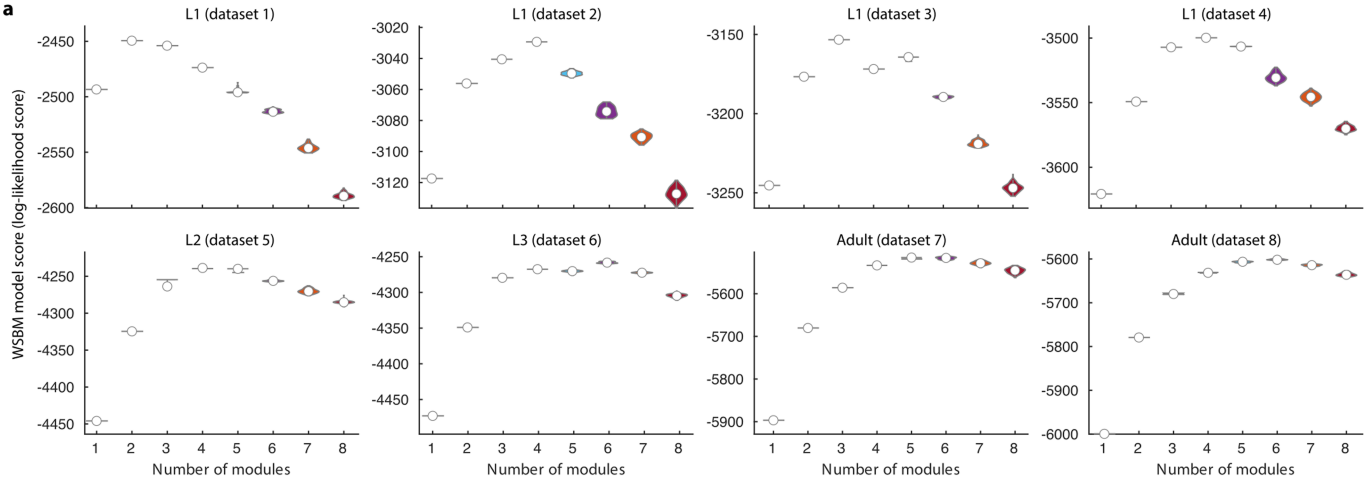

b

Connections included	Dataset 1 (L 1)	Dataset 2 (L 1)	Dataset 3 (L 1)	Dataset 4 (L 1)	Dataset 5 (L 2)	Dataset 6 (L 3)	Dataset 7 (Adult)	Dataset 8 (Adult)
All connections	2	3	3	4	4	6	6	6
Non-variable connections	2	2	2	2	2	4	5	5
Stable connections	2	2	2	2	2	2	2	2

Extended Data Fig. 8 | Cell modules across maturation. a, The log-likelihood score for each WSBM model (Methods). **b**, Optimal number of modules detected by WSBM using subsets of connections.

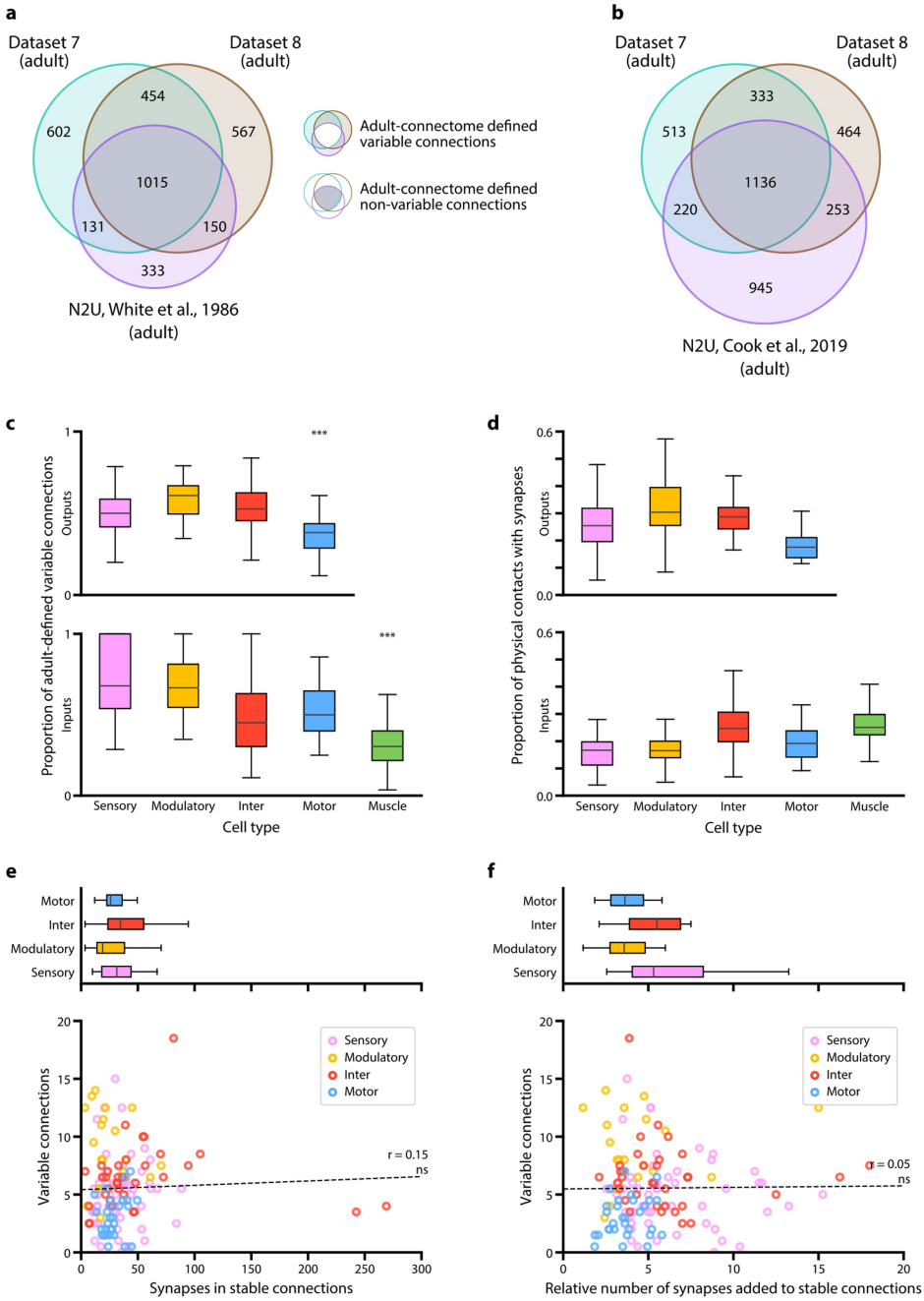

Extended Data Fig. 9 | See next page for caption.

Extended Data Fig. 9 | Comparison of multiple adult connectomes reveals extensive variability in connectivity. a, Shared and unique connections for three adult connectomes: dataset 7, dataset 8, and N2U (a) annotated by White et al. 1986 (ref. [40]), illustrated in the Venn diagram. Connections of all synapse numbers are included for comparison (Methods). **b**, Re-annotation of N2U increased its variability. Re-annotation of the N2U adult connectome (ref. [41]) added 1109 new connections that disproportionally enlarged its pool of unique connections (Methods). Only 16% contributed to connections shared by three connectomes. This suggests the use of different annotation criteria from the original annotation. **c**, Propensity of forming variable connections correlates with cell type. Comparison between the proportion of adult connectome-defined variable and non-variable connections for each cell type. Adult-defined non-variable connections include the connections that are present in both of our adult datasets as well as the original connectome annotated by White et al. 1986. Cell types with significantly higher or lower proportions of variable connections are denoted; upper panel: ***P (sensory-motor) = 5.1×10^{-5}, ***P (modulatory-motor) = 1.7×10^{-6}, ***P (inter-motor) = 7.5×10^{-5}, lower panel: ***P (sensory-muscle) = 2.6×10^{-6}, ***P (modulatory-muscle) = 9.9×10^{-9}, ***P (inter-muscle) = 4.7×10^{-4}, ***P (motor-muscle) = 2.6×10^{-6}; two-sided Mann–Whitney U test, FDR adjusted using Benjamini–Hochberg correction. Centre line, median; box limits, upper and lower quartiles; whiskers, 1.5x interquartile range; outliers not shown. **d**, The low variability of connections from motor neurons to muscles cannot be simply explained by saturation of their physical contacts by synapses. Physical contacts are not saturated for connections for any cell type. Motor neurons, which have the lowest proportion of variable connections (Extended Data Fig. 6j), are not restricted by few available potential synaptic partners. Centre line, median; box limits, upper and lower quartiles; whiskers, 1.5x interquartile range; outliers not shown. **e**, Higher variability for certain cell types is not explained by a fixed probability of an erroneous connection by neurons with abundant synapse formation. Top: the number of synapses for stable output connections by cell types. Modulatory neurons, which exhibit a higher proportion of variable connections than other cell types (Extended Data Fig. 6j), do not exhibit more synapses per stable connection. Centre line, median; box limits, upper and lower quartiles; whiskers, 1.5x interquartile range; outliers not shown. Bottom: The number of variable connections formed by a cell does not correlate with the strength of its stable output connections. Each data point represents one cell. ns (not significant) $P = 0.08$, $r = 0.15$, $n = 139$, two-sided Spearman's rank correlation coefficient. **f**, Top: the relative number of synapses added to existing stable output connections by cell types. Connections from modulatory neurons, which have a higher proportion of variable connections than other cell types (Extended Data Fig. 6j), do not exhibit higher increase in synapse number than connections from other cell types. Centre line, median; box limits, upper and lower quartiles; whiskers, 1.5x interquartile range; outliers not shown. Bottom: The number of variable connections formed by a cell does not correlate with the number of synapses added to existing stable output connections from birth to adulthood. The relative number of synapses added is quantified as the fold increase of synapse number from birth (dataset 1) to adulthood (averaged of datasets 7 and 8). Each data point represents one cell. ns (not significant) $P = 0.56$, $r = 0.05$, $n = 139$, two-sided Spearman's rank correlation coefficient. For panels **d**–**f**, the synapse number for the adult brain (averaged of datasets 7 and 8) is shown.

Extended Data Table 1 | Cell types in the nerve ring

Class	Members	Type	Integration into nerve ring
ADA	2	inter	embryonic
ADE	2	modulatory	embryonic
ADF	2	sensory	embryonic
ADL	2	sensory	embryonic
AFD	2	sensory	embryonic
AIA	2	inter	embryonic
AIB	2	inter	embryonic
AIM	2	modulatory	embryonic
AIN	2	inter	embryonic
AIY	2	inter	embryonic
AIZ	2	inter	embryonic
ALA	1	modulatory	embryonic
ALM	2	sensory	embryonic
ALN	2	sensory	post-embryonic
AQR	1	sensory	post-embryonic
ASE	2	sensory	embryonic
ASG	2	sensory	embryonic
ASH	2	sensory	embryonic
ASI	2	sensory	embryonic
ASJ	2	sensory	embryonic
ASK	2	sensory	embryonic
AUA	2	sensory	embryonic
AVA	2	inter	embryonic
AVB	2	inter	embryonic
AVD	2	inter	embryonic
AVE	2	inter	embryonic
AVF	2	modulatory	post-embryonic
AVH	2	modulatory	embryonic
AVJ	2	modulatory	embryonic
AVK	2	modulatory	embryonic
AVL	1	modulatory	embryonic
AVM	1	sensory	post-embryonic
AWA	2	sensory	embryonic
AWB	2	sensory	embryonic
AWC	2	sensory	embryonic
BAG	2	sensory	embryonic
BDU	2	inter	embryonic
BWM01	4	muscle	embryonic
BWM02	4	muscle	embryonic
BWM03	4	muscle	embryonic
BWM04	4	muscle	embryonic
BWM05	4	muscle	embryonic
BWM06	4	muscle	embryonic
BWM07	4	muscle	embryonic
BWM08	4	muscle	embryonic

Class	Members	Type	Integration into nerve ring
CEP	4	modulatory	embryonic
CEPsh	4	glia	embryonic
DVA	1	modulatory	embryonic
DVC	1	inter	embryonic
FLP	2	sensory	embryonic
GLR	6	glia	embryonic
HSN	2	modulatory	post-embryonic
IL1	6	motor	embryonic
IL2	6	sensory	embryonic
OLL	2	sensory	embryonic
OLQ	4	sensory	embryonic
PLN	2	sensory	post-embryonic
PVC	2	inter	embryonic
PVN	2	modulatory	post-embryonic
PVP	2	inter	embryonic
PVQ	2	modulatory	embryonic
PVR	1	inter	embryonic
PVT	1	inter	embryonic
RIA	2	inter	embryonic
RIB	2	inter	embryonic
RIC	2	modulatory	embryonic
RID	1	modulatory	embryonic
RIF	2	inter	embryonic
RIG	2	inter	embryonic
RIH	1	inter	embryonic
RIM	2	inter	embryonic
RIP	2	inter	embryonic
RIR	1	inter	embryonic
RIS	1	modulatory	embryonic
RIV	2	motor	embryonic
RMD	6	motor	embryonic
RME	4	motor	embryonic
RMF	2	motor	post-embryonic
RMG	2	modulatory	embryonic
RMH	2	motor	post-embryonic
SAA	4	sensory	embryonic
SDQ	2	sensory	post-embryonic
SIA	4	motor	embryonic
SIB	4	motor	embryonic
SMB	4	motor	embryonic
SMD	4	motor	embryonic
URA	4	motor	embryonic
URB	2	sensory	embryonic
URX	2	sensory	embryonic
URY	4	sensory	embryonic

Cell types using each neuron, muscle, and glia that contributed to chemical synapses in our analyses. Cell types assigned using the criteria described in Methods. We performed volumetric reconstructions of all listed neuron and muscle processes within our datasets. We did not perform volumetric reconstructions of the thinner glia processes, which our algorithms were unable to reconstruct automatically (Methods). Volumetric reconstruction of the 6 GLR glia (cells with a mesodermal origin that may affect neuron-muscle communication) and the 4 CEPsh glia (the sheath cells of the cephalic sensilla that have a neuronal/epidermal origin) require thinner electron microscopy sectioning.

nature research

Corresponding author(s): Daniel Witvliet, Jeff Lichtman, Aravi Samuel, Mei Zhen

Last updated by author(s): May 4, 2021

Reporting Summary

Nature Research wishes to improve the reproducibility of the work that we publish. This form provides structure for consistency and transparency in reporting. For further information on Nature Research policies, see our Editorial Policies and the Editorial Policy Checklist.

Statistics

For all statistical analyses, confirm that the following items are present in the figure legend, table legend, main text, or Methods section.

n/a	Confirmed
☐	☒ The exact sample size (*n*) for each experimental group/condition, given as a discrete number and unit of measurement
☒	☐ A statement on whether measurements were taken from distinct samples or whether the same sample was measured repeatedly
☐	☒ The statistical test(s) used AND whether they are one- or two-sided *Only common tests should be described solely by name; describe more complex techniques in the Methods section.*
☐	☒ A description of all covariates tested
☐	☒ A description of any assumptions or corrections, such as tests of normality and adjustment for multiple comparisons
☐	☒ A full description of the statistical parameters including central tendency (e.g. means) or other basic estimates (e.g. regression coefficient) AND variation (e.g. standard deviation) or associated estimates of uncertainty (e.g. confidence intervals)
☐	☒ For null hypothesis testing, the test statistic (e.g. *F*, *t*, *r*) with confidence intervals, effect sizes, degrees of freedom and *P* value noted *Give P values as exact values whenever suitable.*
☐	☒ For Bayesian analysis, information on the choice of priors and Markov chain Monte Carlo settings
☒	☐ For hierarchical and complex designs, identification of the appropriate level for tests and full reporting of outcomes
☐	☒ Estimates of effect sizes (e.g. Cohen's *d*, Pearson's *r*), indicating how they were calculated

Our web collection on statistics for biologists contains articles on many of the points above.

Software and code

Policy information about availability of computer code

Data collection	Neurons were segmented volumetrically in VAST 1.2.1 and skeletonized in CATMAID 2019.06.20
Data analysis	Python 3.6.9 (Pandas 1.1.4, SciPy 1.4.1, Statsmodels 0.12.1), MATLAB R2020b. All code for data analysis is available at github.com/dwitvliet/science-developmental-connectomics

For manuscripts utilizing custom algorithms or software that are central to the research but not yet described in published literature, software must be made available to editors and reviewers. We strongly encourage code deposition in a community repository (e.g. GitHub). See the Nature Research guidelines for submitting code & software for further information.

Data

Policy information about availability of data

All manuscripts must include a data availability statement. This statement should provide the following information, where applicable:

- Accession codes, unique identifiers, or web links for publicly available datasets
- A list of figures that have associated raw data
- A description of any restrictions on data availability

Data collection
Electron microscopy images were aligned in TrakEM2 1.3.2. Neurons were segmented volumetrically in VAST 1.2.1 and skeletonized in CATMAID 2019.06.20

Data analysis
All scripts and files used to generate all figures are available at *https://github.com/dwitvliet/nature2021*.
All data analysis was done in Python 3.6.9 (Pandas 1.1.4, SciPy 1.4.1, Statsmodels 0.12.1) and MATLAB R2020b.

Data availability
All electron microscopy images and volumetric reconstructions are available at *https://bossdb.org/project/witvliet2020*. Connectivity matrices for all datasets are available at *https://www.nemanode.org/* and as Supplementary Tables.

Field-specific reporting

Please select the one below that is the best fit for your research. If you are not sure, read the appropriate sections before making your selection.

☒ Life sciences ☐ Behavioural & social sciences ☐ Ecological, evolutionary & environmental sciences

For a reference copy of the document with all sections, see nature.com/documents/nr-reporting-summary-flat.pdf

Life sciences study design

All studies must disclose on these points even when the disclosure is negative.

Sample size	The number of EM samples was selected to interrogate the developmental time course of maximum nervous system growth and plasticity. The number of adult samples was selected to validate animal-to-animal variability with respect to the one published connectome.
Data exclusions	
Replication	All annotations were replicated by three independent individuals to verify the consistency of each synaptic structure. All samples were drawn from an isogenic population to allow animal to animal comparisons and assess reproducibility.
Randomization	Randomization is not applicable in connectomics as the total number of mapped nervous systems is small.
Blinding	Annotations were done by three individuals working independently and blindly. All results were subsequently collected. Only consistent annotations were reported in analysis.

Reporting for specific materials, systems and methods

We require information from authors about some types of materials, experimental systems and methods used in many studies. Here, indicate whether each material, system or method listed is relevant to your study. If you are not sure if a list item applies to your research, read the appropriate section before selecting a response.

Materials & experimental systems

n/a	Involved in the study
☒	☐ Antibodies
☒	☐ Eukaryotic cell lines
☒	☐ Palaeontology and archaeology
☐	☒ Animals and other organisms
☒	☐ Human research participants
☒	☐ Clinical data
☒	☐ Dual use research of concern

Methods

n/a	Involved in the study
☒	☐ ChIP-seq
☒	☐ Flow cytometry
☒	☐ MRI-based neuroimaging

Animals and other organisms

Policy information about studies involving animals; ARRIVE guidelines recommended for reporting animal research

Laboratory animals	We studied wild-type (Bristol N2) animals reared in standard conditions: 35x10mm NGM-plates, fed by OP50 bacteria, and raised at 22.5 degree C. The animals were within a few generations of the original stock acquired from Caenorhabditis elegans Genetics Center (CGC) in 2001.
Wild animals	The study did not involve wild animals
Field-collected samples	The study did not involve samples collected from the field
Ethics oversight	No ethical considerations needed for working with C. elegans

Note that full information on the approval of the study protocol must also be provided in the manuscript.